Author Manuscript

Author Manuscript

Author Manuscript

Author Manuscript

HHS Public Access

Author manuscript

Nature. Author manuscript; available in PMC 2019 July 22.

Published in final edited form as:

Nature. 2018 November ; 563(7731): 397–401. doi:10.1038/s41586-018-0682-1.

Dopamine enhances signal-to-noise ratio in cortical-brainstem encoding of aversive stimuli

Caitlin M. Vander Weele[1,3], **Cody A. Siciliano**[1,3], **Gillian A. Matthews**[1,3], **Praneeth Namburi**[1], **Ehsan M. Izadmehr**[1], **Isabella C. Espinel**[1], **Edward H. Nieh**[1], **Evelien H.S. Schut**[1,2], **Nancy Padilla-Coreano**[1], **Anthony Burgos-Robles**[1], **Chia-Jung Chang**[1], **Eyal Y. Kimchi**[1], **Anna Beyeler**[1], **Romy Wichmann**[1], **Craig P. Wildes**[1], **Kay M. Tye**[1,*]

[1]The Picower Institute for Learning and Memory, Department of Brain and Cognitive Sciences, Massachusetts Institute of Technology, Cambridge, MA 02139, USA [2]Department of Cognitive Neuroscience, Radboudumc Nijmegen, Nijmegen, The Netherlands [3]Co-first author

Abstract

Despite abundant evidence that dopamine (DA) modulates medial prefrontal cortex (mPFC) activity to mediate diverse behavioral functions[1,2], the precise circuit computations remain elusive. One potentially unifying model by which DA can underlie a diversity of functions is to modulate the signal-to-noise ratio (SNR) in subpopulations of mPFC neurons[3–6], where neural activity conveying sensory information (signal) is amplified relative to spontaneous firing (noise). Here, we demonstrate that DA increases the SNR of responses to aversive stimuli in mPFC neurons projecting to the dorsal periaqueductal gray (dPAG). Using electrochemical approaches, we reveal the precise time course of pinch-evoked DA release in the mPFC, and show that mPFC DA biases behavioral responses to aversive stimuli. Activation of mPFC-dPAG neurons is sufficient to drive place avoidance and defensive behaviors. mPFC-dPAG neurons displayed robust shock-induced excitations, as visualized by single-cell, projection-defined microendoscopic calcium imaging. Finally, photostimulation of DA terminals in the mPFC revealed an increase in SNR in mPFC-dPAG responses to aversive stimuli. Together, these data highlight how mPFC DA can route sensory information in a valence-specific manner to different downstream circuits.

Users may view, print, copy, and download text and data-mine the content in such documents, for the purposes of academic research, subject always to the full Conditions of use:http://www.nature.com/authors/editorial_policies/license.html#termsReprints and permissions information is available at www.nature.com/reprints.

*Correspondence: Kay M. Tye, Ph,D., Picower Institute for Learning and Memory, Department of Brain and Cognitive Sciences, 77 Massachusetts Ave, Bldg-Rm 46-6263, Massachusetts Institute of Technology, Cambridge, MA 01239. kaytye@mit.edu.

AUTHOR CONTRIBUTIONS

C.M.V.W. and K.M.T. conceived the project. C.M.V.W., E.H.N., G.A.M., C.A.S., I.C.E., C.-J.C., P.N. & K.M.T. analyzed data. E.H.N., P.N., C.-J.C., & E.Y.K. provided MATLAB scripts and advice for data analysis. R.W., A.B., C.P.W., & A.B.R. provided technical training. C.M.V.W., C.A.S., G.A.M., E.H.N., & K.M.T. contributed to experimental design. C.M.V.W. and K.M.T. wrote the paper. All authors collected data and contributed to the editing of the manuscript.

K.M.T. is a New York Stem Cell Foundation - Robertson Investigator, a McKnight Scholar and this work was supported by funding from the JPB Foundation, PIIF, PNDRF, JFDP, Klingenstein Foundation, NARSAD Young Investigator Award, New York Stem Cell Foundation, NIH R01-MH102441-01 (NIMH), NIH Director's New Innovator Award DP2-DK-102256-01 (NIDDK), and Pioneer Award DP1-AT009925 (NCCIH). C.M.V.W. and E.H.N were supported by the NSF Graduate Research Fellowship and Integrative Neuronal Systems Training Fellowship (T32 GM007484). C.A.S. is supported by NIH grants F32 MH111216 (NIMH) and K99 DA045103 (NIDA). G.A.M. was supported by the Charles A. King Trust Postdoctoral Research Fellowship Program, Bank of America, N.A., Co-Trustees. R.W. acknowledged funding from the Simons Center and the Netherlands Organization for Scientific Research (NWO) RUBICON. C.A.S., A.B., and R.W. recognize support from the NARSAD Young Investigator Award. Authors declare no competing interests.

Author Manuscript Author Manuscript Author Manuscript Author Manuscript

Despite the popularity of the SNR model for mPFC DA in computational and theoretical neuroscience, the degree to which it translates across brain functions is unknown. Support for DA-mediated SNR has been found in *ex vivo* preparations[4] and *in vivo* during auditory stimulus discrimination[7], visual stimulus discrimination[8], and working memory[9]. Considering mPFC neurons rapidly respond to both rewarding and aversive stimuli[10,11] and that DA neurons in the ventral tegmental area (VTA) projecting to the mPFC (VTA^{DA}-mPFC) are uniquely sensitive to aversive stimuli[12–16], we hypothesized that mPFC neurons encoding aversive or rewarding events are differentially modulated by DA.

Previous characterizations of DA release in the mPFC in response to aversive stimuli have either been direct but slow[14,17] or fast but indirect[12,16]. Fast-scan cyclic voltammetry (FSCV) offers a direct measurement of catecholamine neurotransmission with precise temporal resolution, but is rarely used beyond the striatum due to difficulty in discriminating between norepinephrine (NE) and DA[18]. Here, we investigated the precise time course of DA release using FSCV combined with optical and pharmacological approaches to dissect VTA^{DA} contributions. Electrodes were aimed at deep layers (5-6), where VTA^{DA} terminals were densest, relative to locus coeruleus (LC) NE terminals (LC^{NE}) (Fig. 1a–b), and secured in locations detecting stimulated DA release (Extended Data Fig 1). In tyrosine hydroxylase (TH)::Cre rats expressing halorhodopsin (NpHR) in a Cre-dependent manner in VTA^{DA} neurons, we performed tail pinches with and without photoinhibition of VTA^{DA} neurons (Fig. 1c). Photoinhibition of VTA^{DA} neurons attenuated the pinch-induced signals in the mPFC (Fig. 1d–e). Further, in a separate group of rats, pharmacological inactivation of the LC did not affect pinch-evoked catecholamine release in the mPFC (Extended Data Fig 1). These data suggest that VTA^{DA}-mPFC contributed the bulk of the pinch-evoked, time-locked catecholaminergic signal.

Next, we explored the causal relationship between VTA^{DA}-mPFC and valence processing by testing whether this circuit component was sufficient to induce aversion. In TH::Cre rats, we Cre-dependently expressed channelrhodopsin-2 (ChR2) in VTA^{DA} neurons and implanted optical fibers over the mPFC (Fig. 1f). Activation of VTA^{DA}-mPFC had no effect in real-time place avoidance (RTPA) or conditioned place aversion (CPA) assays (Extended Data Fig. 2). However, in light of the model for DA involvement in enhancing SNR, we considered whether DA might enhance responses to discrete, predictive cues. We trained rats to associate auditory or visual cues (counter-balanced) with either shock or sucrose delivery. Once rats learned to discriminate the cues predicting shock or sucrose by freezing or approaching the sucrose port, respectively (Extended Data Fig. 2), we tested their behavioral responses to the “competition” of simultaneously presented cues (Fig. 1g) driving conflicting motivational outputs[10] (Fig. 1h). Photostimulation of VTA^{DA}-mPFC (using empirically-determined optical parameters, Fig. 1i) during the “competition” trials caused ChR2 rats to spend significantly less time in the sucrose delivery port and more time freezing compared to eYFP controls (Fig. 1j–k). Taken together, these data suggest that DA is released in a time-locked manner upon an aversive stimulus and that VTA^{DA} in the mPFC biases behavioral responses towards aversion in the face of conflicting motivational drives.

Author Manuscript Author Manuscript Author Manuscript Author Manuscript

We next sought to identify distinct, anatomically-defined subpopulations in the mPFC that might relay information relevant to aversive processing. The mPFC has many downstream projection targets, including the periaqueductal gray (PAG) and nucleus accumbens (NAc) (Extended Data Fig. 3). In animal studies, stimulation of the PAG evokes aversive responses, including defensive and attack behaviors[19–21]. While projections to the dorsal PAG (dPAG) have been explored in the context of social behavior[22], contributions of the mPFC-dPAG circuit to discrete stimulus processing have not yet been evaluated. Due to its reported role in reward-related processes, we also investigated the mPFC-NAc projection for comparison[23–25]. Consistent with previous results[22], we found that mPFC-dPAG and mPFC-NAc formed anatomically distinct subpopulations (Extended Data Fig. 3).

To target these pathways, ChR2 or eYFP alone was Cre-dependently expressed in either mPFC-dPAG or mPFC-NAc neurons (Fig. 2a and Extended Data Fig. 4). Photostimulation of mPFC-NAc neurons did not produce detectable differences in behavior between ChR2 and eYFP expressing groups during RTPA or CPA (Extended Data Fig. 4). In contrast, activation of mPFC-dPAG::ChR2 reduced the time spent in the light-paired chamber in both RTPA (Fig. 2b) and CPA (Fig.2c), relative to eYFP controls. In the open field test, which assays locomotor activity and anxiety-related behavior, mPFC-dPAG photostimulation did not affect distance traveled (Fig. 2d) or time spent in the center of the chamber between ChR2- and eYFP-expressing rats (Extended Data Fig. 5). Strikingly, mPFC-dPAG photostimulation produced a robust increase in marble burying and time spent digging (Fig. 2e–h and Supplementary Video 1). The effects in the RTPA and marble burying assays observed upon mPFC-dPAG somata activation were reproduced by activation of mPFC terminals directly in the dPAG (Extended Data Fig. 5).

Thus far, our data show that optogenetic activation of the mPFC-dPAG projection drives place avoidance and defensive behaviors; however, optogenetic activation may not reflect endogenous circuit function. To address this, we investigated the dynamics of individual neurons in the mPFC-dPAG and mPFC-NAc populations during punishment (shock) or reward (sucrose). We performed *in vivo* microendoscopic imaging[26] of neurons expressing a genetically-encoded calcium indicator (GCaMP6m)[27]. GCaMP6m was selectively expressed in mPFC-dPAG and mPFC-NAc neurons (Fig. 3a), to visualize changes in intracellular calcium concentration indicative of neural activity. Assessment of bulk activity revealed that the mPFC-NAc population was not significantly modulated by either shock or sucrose (Fig. 3b). In contrast, mPFC-dPAG neurons showed a robust, time-locked increase in activity in response to foot shock and a decrease in response to sucrose (Fig. 3c). To assess the activity of individual projection-defined neurons, we used a constrained non-negative matrix factorization algorithm optimized for microendoscopic imaging (CNMF-E)[28] (Fig. 3d and Supplementary Video 2 **&** 3). We identified 169 mPFC-NAc and 118 mPFC-dPAG neurons that sorted into 6 functional clusters (Fig. 3e and Extended Data Fig. 6). When comparing the normalized responses of individual cells within each population, mPFC-NAc responses were heterogeneous while mPFC-dPAG responses were robustly biased towards shock (Fig. 3f and Supplementary Video 4 **&** 5). Further, mPFC-dPAG neurons had transients that were both more frequent and higher amplitude during shock sessions, compared to mPFC-NAc neurons (Extended Data Fig. 6).

Author Manuscript Author Manuscript Author Manuscript Author Manuscript

Based on these functional and anatomical differences, we next hypothesized that DA might differentially impact mPFC-NAc and mPFC-dPAG populations. To test whether DA had different effects on the intrinsic excitability of these populations, we performed whole-cell patch-clamp recordings in acute slice preparations of the mPFC containing VTA^{DA}-mPFC::ChR2 terminals and retrogradely-labeled mPFC-dPAG or mPFC-NAc neurons (Fig. 3g). We delivered current steps to evoke intermediate levels of neural firing that were paired with photostimulation of VTA^{DA}-mPFC on interleaved sweeps (Fig. 3h). Photostimulation of VTA^{DA}-mPFC reduced the number of spikes per step for mPFC-NAc neurons, but did not detectably alter the excitability of mPFC-dPAG neurons (Fig. 3i). DA-mediated suppression of mPFC-NAc neurons was blocked by the D2 receptor antagonist raclopride (Fig. 3i). To explore DA receptor localization on mPFC-NAc and mPFC-dPAG neurons, we performed retrograde-labeling of projectors in Drd1a-Cre and Drd2-Cre mice injected with Cre-dependently expressed eYFP. We found that mPFC-NAc projectors expressed both D1 and D2 receptors, whereas mPFC-dPAG projectors largely expressed neither (Extended Data Fig. 7). Since DA did not modulate mPFC-dPAG neurons *ex vivo* and this population did not robustly express DA receptors, we considered the possibility that DA modulates the SNR for incoming sensory information – a function only revealed when such inputs are intact.

To explore this idea, we simultaneously recorded calcium dynamics in mPFC-dPAG neurons while stimulating VTA^{DA} terminals *in vivo*. GCaMP6m was targeted to mPFC-dPAG neurons and DA neurons were transduced with the depolarizing red-shifted opsin, Chrimson[29] or mCherry using a DA transporter (DAT)::Cre mouse (Fig. 4a). VTA^{DA}-mPFC terminals were activated during a 10 min laser ON epoch, flanked by two laser OFF epochs without photostimulation (Fig. 4b). Consistent with the model that DA increases SNR in mPFC-dPAG activity, VTA^{DA}-mPFC stimulation decreased mean calcium event frequency (Fig. 4c and Extended Data Fig. 8) and increased mean event amplitude (Fig. 4d and Extended Data Fig. 8). To demonstrate alterations in SNR, we next explored how DA altered activity in mPFC-dPAG neurons in the presence of aversive signals. To test this, we used ChR2-assisted photoidentification of mPFC-dPAG projectors during electrophysiological recordings, coupled with optical manipulations of VTA^{DA}-mPFC (Fig. 4e). VTA^{DA}-mPFC terminals were stimulated during a 10 min ON epoch flanked by two OFF epochs in an *in vivo* head-fixed preparation[30]. While recording, unpredicted sucrose and airpuff presentations were interleaved and mPFC-dPAG::ChR2 neurons were optically tagged with blue light at the end of the session (Fig. 4f). Of the 204 total mPFC units recorded, 32 were phtotoidentified as mPFC-dPAG projectors using *ex vivo* verified response latencies (Fig. 4g–h). Consistent with our *in vivo* calcium imaging results, a large proportion of mPFC-dPAG neurons were excited to airpuff (Fig. 4i). VTA^{DA}-mPFC stimulation did not change basal firing rates in phototagged or unidentified populations (Extended Data Fig. 9). Examination of time-locked neural activity revealed a selective DA-mediated amplification of airpuff responses (Fig. 4j–l), but not sucrose responses (Fig. 4m–n) in mPFC-dPAG neurons. This increase in SNR was not observed in the unidentified or photoinhibited populations (Extended Data Fig. 10).

Threatening environmental stimuli require immediate disengagement from ongoing behavior and engagement of escape and avoidance strategies, which requires tuning of valence-defined circuits. We speculate that DA in the mPFC primes top-down neural circuits that

Author Manuscript Author Manuscript Author Manuscript Author Manuscript

encode aversive stimuli in order to promote avoidance and escape-related defensive behaviors. These findings have clinical relevance to neuropsychiatric disorders characterized by DA dysregulation in the mPFC. For example in schizophrenia, hyper-dynamic mesocortical DA may prime aversion-encoding pathways and underlie pathologies in paranoid schizophrenia, such as the tendency to assign negative motivational salience to otherwise neutral stimuli. Our data suggest that mesocortical DA governs information routing down discrete mPFC projections and highlights the need for targeted circuit-specific DA therapies in the mPFC.

METHODS

General virus surgery.

Specific subject/surgery details for each experiment are detailed below. For all subjects, surgeries were performed under aseptic conditions and body temperature was maintained with a heating pad. Rodents were anesthetized with isoflurane mixed with oxygen (5% for induction, 2-2.5% for maintenance, 1L/min oxygen flow rate) and placed in a digital small animal stereotax (David Kopf Instruments, Tujunga, CA, USA). Following initial induction, hair was removed from the dorsal surface of the head with hair clippers, ophthalmic ointment was applied to the eyes, the incision area was scrubbed with alcohol pads and betadine (x3 each), and 2% lidocaine was injected just under the skin surface above the skull for topical anesthesia. All measurements were made relative to bregma (unless noted otherwise) for virus/implant surgeries. Viral injections were performed using a beveled microinjection needle (26 gauge for rat; 33 gauge for mice) with a 10 μL microsyringe (Nanofil; WPI, Sarasota FL, USA) delivering virus at a rate of 0.05-0.01 μL/min using a microsyringe pump (UMP3; WPI, Sarasota, FL, USA) and controller (Micro4; WPI, Sarasota, FL, USA). For injections at multiple locations on the dorsal-ventral axis, the most ventral location was completed first and the injection needle was immediately relocated to the more dorsal location for the next injection. After injection completion, 15 min were allowed to pass before the needle was slowly withdrawn. After viral infusions were completed, craniotomies were filled with bone wax and the incision closed with nylon sutures. Subjects were maintained under a heat lamp and provided 0.05 mg/kg (rat) / 0.10 mg/kg (mouse) buprenophine (s.c., diluted in warm Ringers solution) until fully recovered from anesthesia.

All experiments involving the use of animals were in accordance with NIH guidelines and approved by the MIT Institutional Animal Care and Use Committee. For all experiments involving viral or tracer injections, animals containing mistargeted injection(s) were excluded after histological verification.

Viral constructs.

Recombinant AAV_5 vectors carrying ChR2[31,32], NpHR[33,34], or fluorescent proteins (mCherry or eYFP) were packaged by the University of North Carolina Vector Core (Chapel Hill, NC, USA). AAV_8-hSyn-FLEX-ChrimsonR-tdTomato[35] and AAV_5-hSyn-mCherry was packaged by the University of North Carolina Vector Core (Chapel Hill, NC, USA). Viruses carrying GCaMP6m[36,37] were packaged by the University of Pennsylvania Vector Core

Author Manuscript Author Manuscript Author Manuscript Author Manuscript

(Philadelphia, PA, USA). Canine adeno-associated virus[38] carrying Cre recombinase (CAV2-Cre 4.2×10^{12} infectious units/mL) was packaged and obtained from the Istitut de Génétique Moléculaire de Montpellier, France from Dr. Eric Kremer. AAV_9-hEF1a-DIO-synaptophysin-mCherry was packaged from Dr. Rachael Neve at the Viral Gene Transfer Core Facility at MIT (now located at Massachusetts General Hospital).

Catecholamine terminal tracing.

Male heterozygous tyrosine hydroxylase (TH)::Cre mice (8-9 weeks old) received unilateral injections of the anterogradely-traveling adeno-associated virus serotype 5 (AAV_5), encoding the fluorescent protein mCherry or eYFP under a double-floxed inverted open-reading frame (DIO) construct (AAV_5-DIO-EF1a- mCherry or AAV_5-DIO-EF1a-eYFP) in the ventral tegmental area (VTA; AP: −3.4, ML: +0.4, DV: −4.25 [1 μl]) and locus coeruleus (LC; AP: −5.45, ML: 1.25, DV: −4.0 & −7.8 [0.5 μl]), counter-balanced. Mice (n = 3) were given 10 weeks for viral expression and trafficking of the fluorescent protein to terminals in the medial prefrontal cortex (mPFC). After virus incubation, mice were transcardially perfused, and tissue was sectioned and immunohistochemically prepared to label TH+ neurons for histological analyses (described below). For quantification of fluorescently labeled TH+ neurons in the LC and VTA, single Z-stacks in the medial VTA and central LC were acquiring using a scanning confocal microscope (Olympus FV1000) with Fluoview software (Olympus, Center Valley, PA, USA) under a 60x/1.42 NA oil immersion objective. The number of co-labeled (TH+ and eYFP/mCherry+) neurons and eYFP/mCherry only labeled neurons were counted. Z-stack stitches encompassing both prelimbic (PL) and intralimbic (IL) regions of the mPFC were acquired under a 40x/1.30 NA oil immersion objective. Quantification of fluorescence intensity as a proxy for terminal density was accomplished by analyzing 100w x 200h μm sections across mPFC layers based on DAPI density/morphology in FIJI ImageJ. Sections were normalized to the section with peak fluorescence within subjects. Sample size was based on reports in related literature and were not predetermined by calculation.

Fast-scan cyclic voltammetry (FSCV).

Subjects.—Male and female heterozygous BAC transgenic TH::Cre rats[39] (~220 g) were dual housed with *ad libitum* access to water on a normal 12h:12h light/dark cycle (lights on at 09:00 AM).

Surgery.—TH::Cre rats which had received a unilateral injection of 2 μl adeno-associated virus serotype 5 (AAV_5), encoding channelrhodopsin-2 (ChR2)-mCherry or halorhodopsin 3.0 (NpHR)-eYFP, under a double-floxed inverted open-reading frame construct (DIO) (AAV_5-DIO-EF1a-ChR2-mCherry or AAV_5-DIO-EF1a-NpHR-eYFP) in the ventral tegmental area (VTA; AP: −5.3, ML: +0.7, DV: −8.2 & −7.8 [1 μl ea]) were given at least 8 weeks for viral expression before recording. Anesthetized *in vivo* FSCV experiments were conducted similar to those previously described[40,41]. Rats were anesthetized with urethane (1.5 g/kg, i.p.) diluted in sterile saline and placed in a stereotaxic frame located in a faraday cage. For both experiments, a glass-encased carbon fiber electrode (~120 μm exposed carbon fiber, epoxied seal) was lowered into the mPFC (AP: +3.2, ML: +0.8 mm relative to bregma;

Author Manuscript Author Manuscript Author Manuscript Author Manuscript

DV: −2.0 mm from brain surface) through a small craniotomy performed above the deep layers of the mPFC for voltammetric recordings.

For ChR2 experiments (n = 5), additional craniotomies were performed above the VTA (AP: −5.5, ML: −0.6 mm), locus coeruleus (LC; AP: −9.75, ML: −1.25 mm), and contralateral cortex. A Ag/AgCl reference electrode, chlorinated just prior, was implanted in the contralateral cortex. A manually-constructed optical fiber[42] (400 μm core, 0.48 NA; Thorlabs, Newton, NJ, USA) cut to 8 mm in length held in a 2.5 mm ferrule (Precision Fiber Products, Milpitas, CA, USA) was implanted above the VTA (DV: −7.0 mm), and a 26 gauge guide cannula (PlasticsOne, Roanoke, VA, USA) was positioned over the LC (DV: −6.6 mm). Implants were secured to the skull with adhesive cement (C&B Metabond; Parkell, Edgewood, NY, USA).

After cement dried, the optic fiber implant was connected to a patch cable (Doric, Quebec, CA) via a ceramic sleeve (PFP, Milpitas, CA, USA) and both reference and carbon-fiber recording electrode connected to the FSCV interface via custom-made headstage (Scott Ng-Evans, Paul E.M. Phillips Lab, University of Washington, USA). Dopamine (DA) release was evoked by optical activation of the VTA using 150 pulses of 473 nm light (25 mW, 5 ms pulse duration) at 50 or 30 Hz, delivered via a DPSS laser (OEM Laser Systems, Draper, UT) through the attached patch cable and controlled using a Master-8 pulse stimulator (A.M.P.I., Jerusalem, Israel). Electrodes were stereotaxically lowered in 0.2 mm increments until optimal DA release was detected by photoactivation of VTA DA neurons. Optically-evoked DA release was not detected from one subject for unknown reasons; however, tail-pinch evoked catecholamine release was observed with characteristic cyclic voltammograms (CVs) for catecholamines and that rat was therefore included in analyses.

For NpHR experiments (n = 5), craniotomies (in addition to that above the mPFC) were performed above the VTA (AP: −5.5, ML: −0.6 mm), nucleus accumbens shell (NAc, AP: 1.5, ML: +0.9), and contralateral cortex. A Ag/AgCl reference electrode, chlorinated just prior, was implanted in the contralateral cortex and secured to the skull with adhesive cement (C&B Metabond; Parkell, Edgewood, NY). After cement dried, reference and carbon-fiber recording electrodes were connected to FSCV interface via headstage and the recording electrode was stereotaxically lowered into the NAc shell (DV: −6.6 mm relative to brain surface). Following equilibration (see below), a combination bipolar electrical stimulation electrode and 26 gauge guide cannula (PlasticsOne, Roanoke, VA, USA) was stereotaxically lowered above the VTA (DV: −6.5 mm) in 0.2 mm increments until DA release was detected in the NAc by electrical activation of VTA DA neurons via 60 Hz, 60 pulses (biphasic, 200 uA), controlled by an ISO-Flex stimulus isolator (A.M.P.I., Jerusalem, Israel). Following DA detection, the combination electrical stimulation / guide cannula electrode was cemented in place (C&B Metabond; Parkell, Edgewood, NY, USA) slightly dorsal of the VTA and the carbon-fiber recording electrode transferred into the mPFC (DV: −2.0 mm) and allowed to equilibrate. Sample sizes were based on reports in related literature and were not predetermined by calculation.

Data acquisition.—For both experiments, electrodes were allowed to equilibrate for 20 min at 60 Hz and 10 min at 10 Hz. Voltammetric recordings were collected at 10 Hz by

Author Manuscript Author Manuscript Author Manuscript Author Manuscript

applying a triangular waveform (−0.4 V to +1.3 V to −0.4 V, 400 V/s) to the carbon-fiber electrode versus the Ag/AgCl reference implanted in the contralateral cortex[43]. Data were collected in 60 s files with the tail pinch onset occurring 10 s into the file for a duration of 10 s (TarHeelCV, Chapel Hill, NC). Files were collected every 120 s and background subtracted at the lowest current value prior to pinch onset. Evoked signals maintained characteristic CVs for DA/NE[44], with oxidation and reduction peaks at ~+0.65 V and ~−0.2 V, respectively. For ChR2 experiments, 5 tail pinch recordings were obtained with a 120 s inter-recording interval, prior to LC inactivation. After recordings were completed, 1 μl of tetrodotoxin (TTX, 10 ng/1.5 μl artificial cerebral spinal fluid) mixed with fast green (for spread visualization) was injected into the LC via a microinjection needle through the 26 gauge guide cannula controlled by a syringe pump. 2 min following infusion completion, 5 tail pinch recordings were obtained with a 120 s inter-recording interval, post-LC inactivation. For NpHR experiments, recordings were similarly obtained as 10 recordings at 120 s inter-recording interval. Trials were interleaved with no optical manipulation trials ("OFF" trials) and trials where VTA DA neurons were inhibited with 20 s constant 598 nm DPSS laser light (5 mW) delivered by a stripped 200 μm core patch cable (Doric, Quebec, CA) inserted into the combination electrical stimulation / guide cannula located dorsal of the NpHR-expressing VTA DA neurons ("ON" trials). Optical inhibition was initiated 5 s into each "ON" trial (i.e., 5 s prior to tail pinch onset) and remained for 20s (i.e., ending 5 s after tail pinch offset). Oscillatory signals were often observed in the mPFC (however, no such signals were detected in the NAc) and were attenuated by tail pinch and electrical stimulation. Trial averaging alleviated oscillatory interference. Following recording, rats were transcardially perfused and fixed (as described below) and processed using immunohistochemistry for TH immunolabeling to confirm viral expression and implant/recording electrode locations using confocal microscopy. Spread of TTX-fast green was recorded during tissue sectioning on a freezing, sliding microtome.

Data analysis.—Signals were converted to changes in catecholamine concentration using chemometric, principal component regression, and residual analyses using a custom LabView program (Umich CV, Courtesy of Richard Keithley), as previously described[45,46] using *in vivo* optically and electrically-evoked CVs and calibration data obtained from an average of 10 electrodes calibrated in known DA concentrations and pH units as previously described[17]. For quantification of blue light evoked DA, area under the curve (AUC) was calculated during the 5 s pre-stimulation period, compared to the AUC 5 s following the initiation of 20 Hz, 60 pulses laser light. For quantification of tail pinch-evoked DA, AUC was calculated during the 10 s prior to pinch onset, compared to the AUC during the 10 s following pinch onset For comparison of pinch-evoked signals in "ON" and "OFF" trials in NpHR experiments, AUC was calculated during the 30 s period following pinch onset.

VTA^{DA}-mPFC behavioral optogenetic experiments.

Subjects.—Male heterozygous BAC transgenic TH::Cre rats[39] (~220 g) were dual housed with *ad libitum* access to water on a normal 12h:12h light/dark cycle (lights on at 09:00 AM). ~1 week following viral injection surgeries, rats were individually housed with restricted food access (~16-20 g chow / day) for ~10 weeks, but retained *ad libitum* access to

Author Manuscript Author Manuscript Author Manuscript Author Manuscript

water. Sample size was based on reports in related literature and was not predetermined by calculation.

Surgery.—TH::Cre rats which had received a unilateral injection of 2 μl of AAV_5-DIO-EF1a-ChR2-eYFP [n = 6-8] or AAV_5-DIO-EF1a-eYFP [n = 5-7]) in the ventral tegmental area (VTA; AP: −5.3, ML: +0.7, DV: −8.2 & −7.8 [1 μl ea]) were given at least 12 weeks to ensure Cre-specific viral transduction of ChR2 in VTA^{DA} neurons and protein transport to distal terminals in the mPFC. Following incubation, 20G stainless steel cannulae (PlasticsOne, Roanoke, VA) were bilaterally implanted above the mPFC (AP: +3.2-3.6; ML: ±2.0, DV: −2.8; mm relative to bregma at a 15° angle, bilateral). Guide cannulae were secured to the skull with 2-4 skull screws, a layer of adhesive cement (C&B Metabond; Parkell, Edgewood, NY, USA), followed by black cranioplastic cement (Ortho-Jet; Lang, Wheeling, IL, USA) containing gentamicin antibiotic. The implant was allowed to completely dry completely before closure of the incision with nylon sutures. 24G cannulae dummies were inserted into the guide cannulae to present clogging.

General testing procedures.—On each test day, a 400 μm core optical fiber was inserted and attached to the cannulae. Optical fibers extended ~250-500 um beyond the cannulae tips. Rats were then transferred to their behavioral apparatus and connected to patch cords connected to dual-rotating commutators for testing. Real-time place preference / aversion and conditioned place preference / aversion assays were identical to those described below. 473 nm laser light was delivered through the patch cords at 20 Hz, 60 p (5 ms pulses) every 30 s at 20 mW from optic fiber tip. If an optic fiber broke into a guide cannula or if a guide cannula became clogged, the contralateral guide cannula was used for remaining experiments. Manipulated hemispheres were counterbalanced.

Real-time place preference / aversion: Individual food-restricted rats were placed in a Plexiglas arena (24in L x 24in W in x 20in H) and were allowed to freely move between two compartments for 1 hr in a dimly lit room containing constant white noise (Marpac Dohm-DS dual speed sound conditioner, Wilmington, NC, USA). Entry into one half of the chamber resulted in photostimulation (VTA^{DA}-mPFC::ChR2/eYFP = unilateral 20 Hz, 60 p, 5 ms pulses every 30 s, 20 mW; mPFC-dPAG/NAc::ChR2/eYFP = bilateral 20 Hz 5 ms pulses, 12-15 mW, *see below*). Stimulation and no stimulation sides were counterbalanced between animals. Rats were tested on 2 consecutive days and on the second day the stimulation side and no stimulation side were reversed. A video camera positioned directly above the arena tracked and recorded movement using EthoVision XT (Noldus, Wageningen, Netherlands). All data presented are tracked from the “center” of the subject and time spent in each zone was averaged across the 2 testing sessions. In between subjects, the behavioral chamber was thoroughly cleaned with 10% glass cleanser diluted in ddH20.

Conditioned place preference / aversion.—Individual food-restricted rats were placed in a Plexiglas arena (30in L x 15in W in x 25in H) divided into two compartments: one with vertical stripes and the other with horizontal stripes. On day 1 (habituation), rats were allowed to freely move between two compartments for 15 min in a brightly lit room containing constant white noise (Marpac Dohm-DS dual speed sound conditioner,

Author Manuscript Author Manuscript Author Manuscript Author Manuscript

Wilmington, NC, USA). Movement was tracked by an overhead video camera positioned above the arena and time spent in each compartment was calculated using EthoVision XT (Noldus, Wageningen, Netherlands). On day 2 and 3, rats were exposed to conditioning sessions (20 min ea, 1 per day) during which they were confined to one side of the chamber and received optical stimulation (VTA^{DA}-mPFC::ChR2/eYFP = unilateral 20 Hz, 60 p, 5 ms pulses every 30 s, 20 mW; mPFC-dPAG/NAc::ChR2/eYFP = bilateral 20 Hz 5 ms pulses, 12-15 mW, *see below*) or no stimulation (counterbalanced for order and side across animals). On day 4 (test), rats were placed in the chamber and allowed to freely explore both compartments in the absence of optical stimulation. Again, movement was tracked by an overhead video camera positioned above the arena using EthoVision XT (Noldus, Wageningen, Netherlands) and a time difference score was calculated by subtracting the time spent in the stimulation-paired compartment on the habituation day from the time spent in the stimulation-pared compartment on the test day (test[time spent in paired side] – habituation[time spent in paired side]).

Stimulus competition task.—Training and testing procedures were similar to those previously described[47]. Training was performed in standard rat operant chambers (23 × 30 × 40 cm; Med Associates) located within sound-attenuating cubicles. Each chamber was equipped with a red house light, speakers for the delivery of tone cues, a sucrose port that was equipped with an infrared beam for the detection of port entries and exits, a syringe pump to deliver sucrose (30% in cage water), 2 light cues on either side of the sucrose port, and a grid floor for the delivery of electrical shocks. Chambers were wiped down with 70% isopropyl alcohol after each session. Prior to training, rats were pre-exposed to sucrose in their homecage and were magazine trained in the operant boxes (60 min, 20 sucrose deliveries). The first phase of training consisted of Pavlovian reward conditioning where rats learned to associate a 20 s conditioned stimulus (CS^{suc}, either a light cue or tone cue [5 kHz, 80 dB], counter-balanced between subjects) with sucrose delivery into the reward port (30% sucrose, 120 uL/ trial).Sucrose was delivered over 10 s during the cue presentation (5-15 s, relative to CS^{suc} onset). Inter-trial intervals were set to an average of 60 s. If sucrose was not consumed (as detected by the lack of a port entry during the 20 s CS^{suc} presentation), sucrose was immediately removed after cue offset via activation of a vacuum tube located in the sucrose port. Rats were trained on sucrose conditioning for 3 days with each session comprised of 25 trials delivered over ~35 min. The second phase of training consisted of four Pavlovian discrimination sessions where conditioned stimuli predicted sucrose (CS^{suc}) or footshock (CS^{shk}) delivery. During these sessions, the opposite conditioned stimulus (either a light cue or tone cue [5 kHz, 80 dB]) co-terminated with 0.5 s footshock (0.60 mA, 19.5 – 20 s relative to CS^{shk} onset). CS^{suc} and CS^{shk} cues were counterbalanced and presented in a pseudorandom manner. Each sessions consisted of 40 total trials (20 of each trial type) with a variable ~60 s ITI. During sucrose conditioning and discrimination sessions, animals were unilaterally connected to a rotating commutator via a dummy patch cord, but no laser light was delivered.

The third phase was the stimulus competition test sessions. Prior to these sessions, an optical fiber was loaded into a guide cannula, connected to a patch cord, and attached to a rotating commutator, identical to the prior phases. During competition sessions, in addition to CS^{suc}

Author Manuscript Author Manuscript Author Manuscript Author Manuscript

and CS^{shk} trials, competition trials were introduced – in which CS^{suc} and CS^{shk} cues and their respective outcomes were co-presented to evoke conflicting motivation between reward- and fear-associated behaviors. 1 s prior to competition trials (CS^{comp}), the 473 nm laser was triggered (20 Hz, 60 p, 5 ms pulses every 5 s) for the duration of the 20 s compound cue (4 stimulation trains per CS). Each competition session consisted of 60 total trials (20 of each trial type) with a variable ~60 s ITI.

Data analysis.—Sucrose port entries and exits provided a read-out for reward-related behavior (based on % of time in the port during each trial type) and were sampled from infrared beam breaks (Med-PC IV, Med Associates. Freezing, defined as the lack of all movement other than respiration, provided a read-out for aversively-motivated behavior. Videos were sampled using side-profiled infrared cameras at 30 fps and freezing was quantified using an automated custom MATLAB script that calculated frame-by-frame changes in total pixel intensity as an approximation for animal movement. Frame-by-frame motion values were converted into freezing scores using a binary method relative to a motion threshold. This method produced values which are highly correlated with hand-scored measured of freezing[47]. The time spent in the port was subtracted from the freezing quantification, as animals showed little movement while collecting sucrose.

Retrograde cholera toxin-B tracing.

Rats.—Male wild-type Long-Evans rats (~220g; Charles Rivers Laboratories, NC, USA) were dual housed on a normal 12h:12h light/dark cycle (lights on at 09:00 AM). Rats were prepared for stereotaxic surgery as described above using the viral infusion parameters also described above (under *general virus surgery*). Briefly, 500 nl of cholera toxin subunit B (CTB) conjugated to Alexa Fluor-488, 555, or 647[48] (0.1%, Molecular Probes, Eugene, OR, USA) was injected into the dorsal periaqueductal gray (dPAG; AP: −6.6, ML: −0.6; DV: −5.4 mm) and NAc shell (AP: +1.5, ML: +0.95, DV: −7.5 mm) (color counterbalanced between animals). After 7 days, rats were transcardially perfused and histologically prepared. Z-stack stitches encompassing both prelimbic (PL) and intralimbic (IL) regions of the mPFC were acquired using a scanning confocal microscope (Olympus FV1000) with Fluoview software (Olympus, Center Valley, PA, USA) under a 40x/1.30 NA oil immersion objective. Quantification of fluorescence intensity across layers was accomplished by analyzing 200w × 400h μm sections encompassing ventral PL / dorsal IL across mPFC layers based on DAPI density/morphology in FIJI ImageJ. Sections were normalized to the section with peak fluorescence within subjects. For cell quantification, the number of CTB positive and double-positive neurons was counted in both the IL and PL subregions of the mPFC using FluoView software (Olympus, Center Valley, PA). To examine potential projections from the VTA to the dPAG 14 VTA sections were immunstained for tyrosine hydroxylase (TH) (see below) and Z-stacks were captured under a 40×/1.30 NA oil immersion objective. In each stack, 100 DAPI+ cells were identified and the proportion of TH+ and CTB+ cells were counted. Sample size was based on reports in related literature and was not predetermined by calculation.

Mice.—Adult male wild-type C56BL/6 mice (~10 wks; Jackson Laboratory, Bar Harbor, ME) were prepared similarly to methods described above. Briefly, 350 nl of Cholera Toxin

Author Manuscript Author Manuscript Author Manuscript Author Manuscript

subunit B (CTB) conjugated to Alexa Fluor-488, 555, or 647 (Molecular Probes, Eugene, OR, USA) was injected into the dorsal periaqueductal gray (dPAG; AP: −4.2, ML: −0.5; DV: −2.4 mm) and NAc shell (AP: +1.0, ML: +0.75, DV: −4.5 mm) (color counterbalanced between animals). Histological, imaging, and data analyses are the same as previously described.

Projection-specific behavioral optogenetic experiments.

mPFC-dPAG and mPFC-NAc Subjects.—Male wild-type Long-Evans rats (~220g; Charles Rivers Laboratories) were dual housed on a normal 12h:12h light/dark cycle (lights on at 09:00 AM). ~1 weeks following viral injection surgeries, rats were individually housed with restricted food access (~16-20 g chow / day) for ~10 weeks, but retained *ad libitum* access to water. Rats were maintained on food restriction unless noted otherwise.

Surgery.—For projection-specific targeting for behavioral optogenetic, male wild-type Long-Evans rats were bilaterally injected with 1.2 μL of AAV_5-Ef1a-DIO-ChR2(H134R)-eYFP in the mPFC at 2 locations along the dorsal-ventral axis (0.6 μL each) (AP: +3.2; ML: ±0.75; DV: −3.5 and −2.5; mm relative to bregma). To achieve projection-specific recombination, retrogradely traveling canine adeno-associated (CAV) virus carrying Cre-recombinase (CAV2-Cre; 4.2×10^{12} infectious units/mL; Institut de Genetique Moleculaire de Montpellier, France) was bilaterally injected (0.6 μL each) in the dorsal periaqueductal gray (dPAG) (AP: −6.0; ML: ±0.6; DV: −5.2; mm relative to bregma [0.4 ul]), or nucleus accumbens (NAc) (AP: +1.4; ML: ±1.0; DV: −7.4; mm relative to bregma [0.5 μL]). A subset of mPFC-dPAG rats were co-injected with 0.1 ul of AAV^5-hSyn-mCherry to visualize virus spread. ~7 days following virus surgery, rats were individually housed and placed on food restriction. ~10 weeks later, manually constructed optic fibers (400 μm core, 0.48 NA) (Thorlabs, Newton, NJ, USA) held in a 2.5 mm ferrule (Precision Fiber Products, Milpitas, CA, USA) were implanted directly above ChR2/eYFP-expressing mPFC neurons projecting to either the dPAG or NAc for projection-specific manipulations (AP: +3.2-3.6; ML: ±1.5, DV: −2.8; mm relative to bregma at a 10° angle, bilateral).

For terminal manipulations, AAV_5-CaMKIIa-ChR2-eYFP was bilaterally injected into the mPFC at 2 locations along the dorsal-ventral axis (0.6 μL each) (AP: +3.2; ML: ±0.75; DV: −3.5 and −2.5; mm relative to bregma). ~7 days following surgery, rats were individually housed and placed on food restriction. ~10 weeks later, manually constructed optic fibers (400 μm core, 0.48 NA) (Thorlabs, Newton, NJ, USA) held in a 2.5 mm ferrule (Precision Fiber Products, Milpitas, CA, USA) were bilaterally implanted directly above the dPAG for mPFC terminal manipulations (AP: −6.6, ML: ±1.5, DV: −4.3 mm relative to bregma at a 10° angle, bilateral). For both experiments, optical fibers were secured to the skull with 2-4 skull screws, a layer of adhesive cement (C&B Metabond; Parkell, Edgewood, NY, USA), followed by black cranioplastic cement (Ortho-Jet; Lang, Wheeling, IL, USA) containing gentamicin antibiotic. The implant was allowed to completely dry before closure of the incision with nylon sutures.

Behavioral testing.—Testing was performed at ~13 wks following viral injection and ~10 days after optical fiber implantation to allow sufficient time for transgene expression and

Author Manuscript Author Manuscript Author Manuscript Author Manuscript

tissue recovery. Throughout this period, rats were maintained on food-restriction (~16-20 g chow / day). Rats were tested during their light phase (09:30 AM – 07:00 pm) under food-deprived conditions. Optic fiber implants were connected to a 200 um patch cable (Doric, Québec, Canada) using a ceramic sleeve (PFP, Milpitas, CA), which connected to a bilateral commutator (rotary joint; Doric, Québec, Canada) by means of an FC/PC adapter to allow unrestricted movement. A second patch cable, with an FC/PC connector at either end (Doric, Québec, Canada), connected the commutator to a 473 nm diode-pumped solid state (DPSS) laser (OEM Laser Systems, Draper, UT). A Master-8 pulse stimulator (A.M.P.I., Jerusalem, Israel) was used to control the output of the 473 nm laser, with a light power of ~10-15 mW (adjusted to account for optic fiber efficiency). Following each day's experimentation, rats were provided their ~16-20 grams of standard

Open field test: Individual food-restricted rats were placed in a Plexiglas arena (24l x 24w x 20h in) and were allowed to move freely within the arena for 9 min with light stimulation occurring during the middle 3 min (3 min OFF, 3 min ON, 3 min OFF design) (mPFC-dPAG/NAc::ChR2/eYFP = bilateral 20 Hz 5 ms pulses, 12-15 mW). The room was brightly lit and contained constant white noise (Marpac Dohm-DS dual speed sound conditioner, Wilmington, NC, USA). A video camera positioned directly above the arena tracked and recorded movement using EthoVision XT (Noldus, Wageningen, Netherlands). In order to assess anxiety-related behavior, the chamber was divided into a center (40 × 40 cm) and periphery region. In between subjects, the behavioral chamber was thoroughly cleaned with 3% acetic acid diluted in ddH20. All data presented are tracked from the "center" of the subject.

Marble burying.—Individual food-restricted rats were placed in a standard, rectangular rodent cage (33w x 40l x 20h cm) containing ~7.5 cm of clean standard bedding and 16 black marbles, which was slightly elevated from the floor (1 m). 16, 1.3 cm diameter black marbles were placed on top of the even bedding in a 4 × 4 array separated from the cage sides by ~5 cm. Rats were tested across 2 days for 12 min each, counter-balanced for laser stimulation (mPFC-dPAG::ChR2/eYFP = bilateral 20 Hz 5 ms pulses, 12-15 mW) in a brightly lit room containing constant white noise (Marpac Dohm-DS dual speed sound conditioner, Wilmington, NC, USA). Behavior was recorded via a video camera positioned directly above the arena using Ethovision XT (Noldus, Wageningen, Netherlands). Photographs of the behavioral arena before (undisturbed) and after each 12 min session were obtained and marbles that were 100% buried were counted. Time spent digging was scored by two experimenters blind to condition using ODLog (Macropod). Cage exploration time was obtained by subtracting the time spent of scored behaviors from the total session length. The time spent engaging in each behavior was quantified by taking the average between the two experimenters. One mPFC-dPAG::ChR2 video was corrupted and was not included in analyses. In between subjects a new cage containing fresh bedding was used and marbles were cleaned with 15% isopropyl alcohol diluted in ddH20.

Following the conclusion of experiments, a subset of rats were stimulated for 5 min in a dark, sound-attenuating room (473 nm, 20 Hz, 20 mW, 5 ms pulses) for c-Fos quantification to verify light-evoked activity in ChR2+ mPFC-dPAG neurons. 80 mins later, rats were

Author Manuscript Author Manuscript Author Manuscript Author Manuscript

deeply anesthetized and transferred to the lab and transcardially perfused. Sample size was based on reports in related literature and were not predetermined by calculation.

In vivo epifluorescent calcium imaging

Projection-specific subjects.—Male wild-type C57BL/6 mice (~8 wks old; mPFC-dPAG::GCaMP6m and mPFC-NAc::GCaMP6m) or male DAT::IRES-Cre mice[49] (~ 8 wks old; mPFC-dPAG::GCaMP6m + VTA^{DA}::ChrimsonR or mCherry) were group housed (2-4 subjects per cage) on a 12h:12h reverse light/dark cycle (lights off at 09.00 AM) prior to and 4 weeks following initial virus and microendoscope (i.e., GRIN lens) implant surgery. Following baseplate adhesion, subjects were individually housed and placed on food restriction (3-6 grams normal chow / day) with *ad libitum* access to water for 3-6 days encompassing testing. Sample sizes were based on reports in related literature and were not predetermined by calculation.

Surgeries.—Subjects were prepared for *in vivo* epifluorescent calcium imaging[50] similarly to methods described elsewhere[51,52]. Briefly, to achieve projection-specific imaging, a virus encoding Cre-dependent GCaMP6m (AAV_5-CAG-Flex-GCaMP6m) was injected into the mPFC (AP: +1.8, ML: +0.3, DV: −2.75 & −2.4 [300 nl ea, bevel facing lateral]) and retrogradely traveling canine adeno-associated (CAV) virus carrying Cre-recombinase (CAV2-Cre; Institut de Génétique Moléculaire de Montpellier, France) was injected into the dPAG (n = 6; AP: −4.2, ML: +0.5, DV: −2.4 [350 nl]) or the nucleus accumbens shell (n = 5; AP: +1.0, ML: +0.75; DV: −4.5 [350 nl]). For manipulation of DA terminals in mPFC-dPAG::GCaMP6m + VTA^{DA}::ChrimsonR subjects (n = 4), DAT::IRES-Cre mice received 1 ul of AAV_8-hSyn-FLEX-ChrimsonR-tdT in the VTA (AP: −3.4, ML: +0.4, DV: −4.25). Control mice (mPFC-dPAG::GCaMP6m + VTA^{DA}::mCherry; n = 5), received 1ul of AAV_5-DIO-EF1a-mCherry into the VTA using the same coordinated. After virus infusions, the mPFC craniotomy was enlarged to >1 mm in diameter and dura removed with a bent 30 gauge beveled needle, but no tissue was aspirated. A 1 mm diameter, ~4 mm length gradient refractive index lens (GRIN lens; GLP-1040, Inscopix, Palo Alto, CA) was held via vacuum on the tip of a blunted needle surrounded by plastic tubing for stability and was lowered stereotaxically through the craniotomy under constant saline perfusion to minimize tissue/blood desiccation. Lenses were implanted slightly posterior and lateral of the needle track for virus infusions to avoid tissue damage in the imaging plane, and were lowered to locations in the ventral PL / dorsal IL subregion of the mPFC (AP: −1.77, ML: −0.4, DV: −2.32, mm from bregma). Lens implants were secured to the skull with a thin layer of adhesive cement (C&B Metabond; Parkell, Edgewood, NY, USA), followed by black cranioplastic cement (Ortho-Jet; Lang, Wheeling, IL, USA) containing gentamicin antibiotic. Lenses were covered with the top of an eppendorf tube and cemented in place with cranioplastic cement for protection during the virus incubation period (3-4 wks). The implant was allowed to completely dry before closure of the incision with nylon sutures.

Following virus incubation, mice were again anesthetized with isofluorane, streotaxically secured, and baseplates (Inscopix, Palo Alto, CA) were cemented around the lens to support the connection of the miniaturized microscope for *in vivo*, freely moving imaging. During this procedure, the protective eppendorf cap and supporting cranioplastic cement were

Author Manuscript Author Manuscript Author Manuscript Author Manuscript

removed using a hand drill. The exposed top of the GRIN lens was scrubbed clean with a cotton-tipped applicator soaked with 15% isopropyl alcohol diluted in ddH_20. Next, a miniaturized microscope (single channel epifluorescence, 475 nm blue LED, Inscopix, Palo Alto, CA) with the baseplate attached was stereotaxically positioned over the implanted GRIN lens and adjusted in the DV axis in order to focus on visible landmarks (i.e., GCaMP6m expressing neurons and blood vessels). After the focal plane was identified, the microscope/baseplate was raised by ~50 um, to account for cement shrinkage, and was subsequently cemented in place with pink dental cement (Stoelting, Wood Dale, IL, USA). The microscope was then detached from the baseplates, a final layer of black cranioplastic cement (Ortho-Jet; Lang, Wheeling, IL, USA) was applied to prevent light leak, and the implant was covered with a protective plate (Inscopix, Palo Alto, CA) until imaging.

Behavioral sucrose/shock paradigm and data acquisition.—Following recovery (~7 days), mice were individually housed and food restricted for 2 days and exposed to 30% sucrose solution (diluted in standard tap/cage H20) in the homecage. Food-deprived mice were then trained in operant chambers equipped with sucrose lickometers (Med Associates, St Albans, VT), with a modified spout that extended into the chamber from the recessed opening, for ~60 min while connected to a plastic “dummy” microscope for training and habituation. All animals readily self-administered sucrose via the lickometer after 2 days of training. On the testing day, food-deprived mice were gently restrained and connected with the miniaturized microscope (single channel epifluorescence, 475 nm blue LED, Inscopix, Palo Alto, CA) via the baseplate and secured with a small screw on the baseplate. Mice were allowed to recover from restraint for 10 min before the first session was initiated. Mice were exposed to two 15-minute imaging sessions (“sucrose” and “shock”), counter-balanced and separated by a 15 min intermediate epoch, during which the animal remained in the chamber, but no sucrose or footshocks were administered. During “sucrose” sessions, food deprived mice were allowed to self-administer sucrose for 15 min via the lickometer they had been exposed to previously. During “shock” sessions, mice were exposed to 27 mild electric food shocks (0.2 mA; 1 s duration; 10-60 inter-shock interval) for 15 min. Gray scale tiff images were collected at 20 frames per second using 20-60% of the miniaturized microscope’s LED transmission range (nVista HD V2, Inscopix, CA).

Recording from mPFC-dPAG neurons while manipulating VTA^{DA} terminal activity.—Following recovery, DAT::Cre mice were individually housed and food restricted for 2 days prior to recording. Prior to the recording day, food-deprived mice were habituated to handling and the nVoke miniaturized microscope (an integrated imaging and optogenetics system, 450 nm blue GCaMP excitation LED, 620 nm amber optogenetic LED, Inscopix, Palo Alto, CA). 24 hrs prior to recordings, mice were habituated in their homecage to a dimly lit recording room containing constant white noise (Marpac Dohm-DS dual speed sound conditioner, Wilmington, NC, USA). On the recording day, mice were attached to the nVoke miniaturized microscope and habituated in their homecage for 15 min. After the 15 min habituation, a 30 min recording session, composed of 10 min OFF-ON-OFF epochs, was initiated. Gray scale images were collected at 10 frames per second using 0.094-0.266 mW / mm^2 (estimated light power based on GRIN lens efficiency) of the miniaturized microscope’s 450 nm LED transmission range (nVoke 2.1.5., Inscopix, Palo Alto, CA).

Author Manuscript Author Manuscript Author Manuscript Author Manuscript

During the ON epoch, 20 Hz, 60p (5 ms pulses) trains of 620 nm LED light were initiated every 30 s for the duration of the 10 min epoch.

Image processing.—Image processing was accomplished using Mosaic software (Version 1.1.2., Inscopix, Palo Alto, CA). Raw videos were pre-processed by applying x4 spatial downsampling to reduce file size and processing time, and isolated dropped frames were corrected. No temporal downsampling was applied. For sucrose/shock experiments, both recordings per animal (i.e., "Sucrose" recording and "Shock" recording) were concatenated to generate a single 30 min video. Lateral movement was corrected for by using a portion of a single reference frame (typically a window surrounding a prominent blood vessel or constellation of bright neurons), as previously described[50,53]. Images were cropped to remove post-registration borders and sections where cells were not observed. 2 methods were used for ROI identification and single-cell fluorescence trace extraction in order to verify that these processes did not significantly change the pattern of results within our data sets. Both methods are described below in *CNMF-E analyses* (with and without non-negative constraint on temporal components) and *non-ROI analyses.* The results from the CNMF-E analyses with non-negative constraint are reported in **Main** Fig. 3 and **Main** Fig. 4. The results from the CNMF-E analyses without non-negative constraint and non-ROI analyses are reported in Extended Data Fig. 6 and Extended Data Fig. 8.

CNMF-E analyses.—After motion correction and cropping, recordings were exported as .tif z-stacks and were downsampled to 10 frames per second. We used a constrained non-negative matrix factorization algorithm optimized for micro-endoscopic imaging (CNMF-E)[54] to extract fluorescence traces from ROIs. ROIs were defined by manually selecting seed pixels from peak-to-noise (PNR) graphs of the FOV[55]. Considering calcium fluctuations can exhibit negative transients, associated with a pause in firing[13,56], we also performed analyses where we did not constrain temporal components to > 0 – these data are provided in the Extended Data Figures.

Non-ROI analyses.—After motion correcting and cropping, recordings were converted to a changes in fluorescence compared to background fluorescence (F-F0)/F0 using the mean Z-projection image of the entire movie as reference (F0). Calcium signals arising from individual regions of interest (ROIs, i.e., cells) were identified using independent and principal component analyses (PCA/ICA), as previously described[57]. Identified PCA/ICA filters were thresholded at their half-max values to define possible ROIs. ROIs were then screened for neuronal morphology and only accepted if the thresholded filters included only one contiguous region with an eccentricity of <0.85 and an area between 30-350 pixels. Accepted ROI filters were merged if their areas overlapped by more than 60% after visual confirmation. The accepted ROI filters were then reapplied to the motion corrected videos to extract dF/F0 traces for each ROI. In order to correct for bleaching and possible neuropil contamination of the extracted ROI trace, we correct each ROI tracing using signals from the whole field, using a multiple step procedure: The full ROI trace and the signals from the whole field were filtered using a 30 s median filter to eliminate the influence of sharp transients or outliers. The influence of the surrounding signals on the ROI trace were quantified using regression (*glmfit* in MATLAB). The resulting regression coefficient was

Author Manuscript Author Manuscript Author Manuscript Author Manuscript

then applied to the original, unfiltered trace to regress out the influence of the non-ROI thresholded field on the ROI trace itself. Multiple background subtraction methods were examined and a non-ROI thresholded approach was implemented because 1) this approach excludes subtraction of prominent processes (i.e., dendrites and axons) observed in our data set, 2) the reasonable correlation coefficients obtained between individual ROIs are consistent with the range that would expected based on electrical recordings. To acquire the non-ROI thresholded image for background subtraction, max Z-projections of individual recordings were created and thresholded to separate ROIs and their processes from the rest of the field of view. Average signal from the remaining pixels was used as a proxy for the whole field changes in fluorescence, and regressed from the signal from each ROI.

Data analysis.—Individual lick bouts were characterized by lick events detected at the sucrose lickometer and events that were separated by >1 s were identified as an individual lick bout. Calcium signals for the bulk FOV fluorescence and for each ROI were aligned to behavioral events (i.e., lick bout initiation and shock). Population z-scores were calculated using the period −10 to −5 s prior to stimuli onset as baseline. ROIs were classified as being stimulus excited if the average z-score 0-1 s after stimulus onset was greater than 3.

For agglomerative clustering, we first concatenated individual neuron's average response aligned to shocks across trials (expressed as **r**(shocks), in Z-score), and its average response aligned to licks across trials (expressed as **r**(licks), in Z-score), such that each row in the heatmap corresponds to one neuron. There were 118 neurons from the PAG and 169 neurons from the NAc in total. Agglomerative hierarchical clustering was applied using Ward's Euclidean linkage, followed by a soft normalization: for each neuron, if its maximum absolute Z-score was above 1, its Z-score at each frame was divided by its maximum Z-score across time. If its maximum absolute Z-score was below 1, it remained unchanged. Pairs of neurons that were in close proximity were linked. As they were paired into binary clusters, the newly formed clusters were grouped into larger clusters until a hierarchical tree was formed. A a threshold at 0.3 × max(linkage) was set to prune branches off the bottom of the hierarchical tree, and assign all the neurons below each cut to a single cluster. After clusters were constructed, data from the PAG and the NAc separated to generate their individual heatmaps using their original average response profiles (without normalization). For both areas, clusters were sorted in an ascending order based on their third quartile of the response to the Shocks. Within each cluster, neurons were also sorted in an ascending order based on their response to the Shocks. Different bars on the left side of the heatmaps corresponds to different clusters. Same color suggests that they belong to the same cluster from the dendrogram. Calcium event quantifications (number and amplitude) were performed in MiniAnalysis (Synaptosoft, Decatur, GA) using individual ROI traces from the entire session after conversion to z-score. Baseline from the z-transform was computed by thresholding the signal at 20% of the signal amplitude. Calcium events with z-scores <5 or that did not have a > 0.5 AUC were not included in analyses because events of this magnitude were not reliably retain transient, calcium-event characteristics across animals. ROIs which did not contain events that meeting event criterion were excluded.

Author Manuscript Author Manuscript Author Manuscript Author Manuscript

Ex vivo electrophysiology to examine dopamine effects on projector populations.

Subjects.—Male and female heterozygous BAC transgenic TH::Cre rats (~220 g; Charles Rivers Laboratories) were dual housed on a normal 12h:12h light/dark cycle (lights on at 09:00 AM) throughout the duration of experiments. Sample sizes were based on reports in related literature and were not predetermined by calculation.

Surgery.—Rats first received bilateral infusions of AAV_5-EF1a-DIO-ChR2-eYFP, as previously described (*FSCV Surgeries*). Rats were allowed to recover for virus surgery for an 8-10 weeks incubation period to ensure Cre-specific viral transduction of ChR2 in VTA^{DA} neurons and protein transport to distal terminals in the mPFC. After incubation, rats received a second surgery to retrogradely label dPAG and NAc shell projectors in the mPFC. CTB injections were performed similarly as previously described (*Retrograde cholera toxin-B tracing*). Briefly, rats received bilateral injections of CTB conjugated to Alexa Fluor-488 or −555 (Molecular Probes, Eugene, OR, USA) into the dPAG (AP: −6.6, ML: −0.6; DV: −5.4 mm), the NAc (AP: +1.5, ML: +0.95, DV: −7.5 mm), or one in each hemisphere (fluorophores were counterbalanced between rats).

Brain slice preparation.—7 days following CTB injections, TH::Cre rats were deeply anesthetized with sodium pentobarbital (250 mg/kg; IP) and transcardially perfused with 60 mL ice cold modified artificial cerebrospinal fluid (aCSF) (NaCl 87, KCl 2.5, NaH2PO4*H20 1.3, MgCl2*6H2O 7, NaHCO3 25, sucrose 75, ascorbate 5, CaCl2*2H2O 0.5 [composition in mM] in ddH20; osmolarity 322-326 mOsm, pH 7.20-7.30) saturated with carbogen gas (95 % oxygen, 5 % carbon dioxide). Following decapitation, the brain was rapidly removed from the cranial cavity and coronally dissected (AP: ~ −1.5 mm from bregma). Coronal 300 μm brain sections were prepared from the anterior portion of the brain containing the mPFC and striatum, using a vibrating microtome (Leica VT1000S, Leica Microsystems, Germany). The posterior portion of the brain was transferred to 4% paraformaldehyde (PFA) dissolved in 1x PBS for fixation and subsequent histological processing (see below in Histology). Brain slices were given at least 1 hr to recover in a holding chamber containing aCSF (NaCl 126, KCl 2.5, NaH2PO4*H20 1.25, MgCl2*6H2O 1, NaHCO3 26, glucose 10, CaCl2*H2O 2.4 [composition in mM]; in ddH20; osmolarity 298-301 mOsm; pH 7.28-7.32) saturated with carbogen gas at 32 °C before being transferred to the recording chamber for electrophysiological recordings.

Whole-cell patch-clamp recordings.—Once in the recording chamber, brain slices were continually perfused with fully oxygenated aCSF at a rate of 2 mL/min at 30-32 °C. Neurons were visualized using an upright microscope (Scientifica, Uckfield, UK) equipped with IR-DIC optics and a QImaging Retiga EXi camera (QImaging, Surrey, BC, Canada) through a 40X water-immersion objective. Brief illumination through a 470 nm or 595 nm LED light source (pE-100; CoolLED, Andover, UK) was used to identify CTB-488 and CTB-555 expressing mPFC neurons, respectively, prior to recording. Whole-cell patch-clamp recordings were performed using glass electrodes (resistance 4-6 MΩ) pulled from thin-walled borosilicate glass capillary tubing (World Precision Instruments, Hertfordshire, UK) on a P-97 horizontal puller (Sutter Instrument, Novato, CA, USA) and filled with internal solution containing (in mM) potassium gluconate 125, NaCl 10, HEPES 20, Mg-

Author Manuscript Author Manuscript Author Manuscript Author Manuscript

ATP 3, neurobiotin 0.1 % in ddH20 (osmolarity 287, PH 7.33). For electrophysiological recordings signals were amplified using a Multiclamp 700B amplifier (Molecular Devices, CA, USA), digitized at 10 kHz using a Digidata 1550 (Molecular Devices, CA, USA), and recorded using Clampex 10.4 software (Molecular Devices, CA, USA). Capacitance, series resistance (R_s), and input resistance (R_{in}) were frequently measured during recordings to monitor cell health, using a 5 mV hyperpolarizing step in voltage-clamp. The resting membrane potential and the current-voltage (I-V) relationship of the neuron were determined in current-clamp mode using incremental 20 pA, 500 ms square current pulses from −120 pA to +260 pA. The instantaneous and steady-state action potential firing frequencies were calculated using the first 100 ms and last 300 ms of the current pulse, respectively.

In order to assess the effect of activating ChR2-expressing VTA (DA) terminals on mPFC neuron firing, a square current pulse (2 s duration) was applied in current-clamp mode to elicit stable firing (~2-6 Hz). After 20 s a 20 Hz train of 470 nm light (5 ms pulse duration) was delivered through the 40X objective for 3 s. During the last 2 s of this blue light train, the same square current pulse was applied to the cell. This protocol was repeated every 50 s and the firing during the current pulses (with and without blue light stimulation) was used for analysis. To determine the effect of VTA (DA) terminal stimulation on the rheobase of the neuron, the same protocol was performed, but instead of a square current pulse, a 2 s current ramp was applied to the cell.

The D_2 antagonist raclopride was used in a subset of recordings during which a square current pulse was applied with and without optical stimulation of ChR2-expressing VTA (DA) terminals. Raclopride (Sigma-Aldrich, MO, USA) was prepared fresh at the start of each recording session and was dissolved in aCSF to give a final concentration of 10 μM. Raclopride was perfused onto the slice for at least 10 min before electrophysiological recordings were commenced.

Analysis of action potential firing was performed offline using Clampfit 10.4 software (Molecular Devices, Sunnyvale, CA) and passive membrane properties were computed using custom MATLAB software written by Praneeth Namburi based on MATLAB implementation of the Q-method[58].

Immunohistochemistry.—Following recording, slices were transferred to 4% PFA solution overnight at 4 °C, and were then washed 4 times (for 10 min each) in 1x PBS. Slices were then blocked in 1x PBS solution containing 0.3% Triton X-100 and 5% normal donkey serum (NDS; Jackson ImmunoResearch, PA, USA) for 1 h at room temperature. They were then incubated in primary antibody solution containing chicken anti-TH (1:1000; Millipore, MA, USA) in 1x PBS with 0.3% Triton X-100 (Thermo Fisher Scientific, MA. USA) and 3% NDS overnight at 4 °C. Slices were subsequently washed 4 times (for 10 min each) in 1x PBS and then incubated in secondary antibody solution containing Alexa Fluor 647-conjugated donkey anti-chicken (1:1000; Jackson ImmunoResearch, PA, USA) and 405-conjugated streptavidin (1:1000; Biotium, CA, USA) in 1x PBS with 0.1% Triton X-100 and 3% NDS for 2 h at room temperature. Slices were finally washed 5 times (for 10

Author Manuscript Author Manuscript Author Manuscript Author Manuscript

min each) in 1x PBS, then mounted onto glass slides and cover-slipped using polyvinyl alcohol (PVA) mounting medium with DABCO (Sigma-Aldrich, MO, USA).

Ex vivo electrophysiology to determine latency for phototagging experiments.

Subjects & surgery.—To verify the latency of blue light-evoked action-potentials (AP) in ChR2-expressing mPFC-dPAG projectors, DAT::Cre mice were used which had received the same viral surgery as those for *in vivo* electrophysiology experiments. Viral incubation for *ex vivo* recordings was matched for those for *in vivo* experiments. For subject and surgery details, see below in vivo electrophysiology.Surgery

Brain slice preparation.—Brian slice preparation was similar to previously descriped. Briefly, mice were deeply anesthetized with sodium pentobarbital (90 mg/kg; IP) and transcardially perfused with 20 mL ice cold modified artificial cerebrospinal fluid (aCSF) (NaCl 87, KCl 2.5, NaH2PO4*H20 1.3, MgCl2*6H2O 7, NaHCO3 25, sucrose 75, ascorbate 5, CaCl2*2H2O 0.5 [composition in mM] in ddH20; osmolarity 322-326 mOsm, pH 7.20-7.30) saturated with carbogen gas (95 % oxygen, 5 % carbon dioxide). Following decapitation, the brain was rapidly removed from the cranial cavity and coronally dissected (AP: ~ 0 mm from bregma). Coronal 300 μm brain sections were prepared from the anterior portion of the brain containing the mPFC and striatum, using a vibrating microtome (Leica VT1000S, Leica Microsystems, Germany). The posterior portion of the brain was transferred to 4% paraformaldehyde (PFA) dissolved in 1x PBS for fixation and subsequent histological processing (see below in Histology). Brain slices were given at least 1 hr to recover in a holding chamber containing aCSF (NaCl 126, KCl 2.5, NaH2PO4*H20 1.25, MgCl2*6H2O 1, NaHCO3 26, glucose 10, CaCl2*H2O 2.4 [composition in mM]; in ddH20; osmolarity 298-301 mOsm; pH 7.28-7.32) saturated with carbogen gas at 32 °C before being transferred to the recording chamber for electrophysiological recordings.

Whole-cell patch clamp recordings.—Recordings were similar to those previously described above. Briefly, recordings were made from visually identified neurons expressing ChR2-eYFP and non-expressing neighbors. Blue light was provided by a 470 nm LED light source (pE-100; CoolLED, NY, USA) delivered through a 40X immersion objective. ChR2 expresison in recorded neurons was confirmed by the presence of sustained inward current in response to 1 s constant pulse of blue light delivered in voltage-clamp mode.

Offline analysis was performed in Clampfit 1.4 software (Molecular Devices, Sunnyvale, CA). Latency to AP or excitatory postsynaptic potentials (EPSP) were peak averaged from 30 responses to a 5 ms pulse of blue light (delivered in a 10 pulse, 1 Hz train every 60 s). Latency was measured as the durations from the onset of the light pulse to the peak of the AP or EPSP.

Dopamine receptor localization on projector populations.

Subjects.—Transgenic male and female Drd1a-Cre [n = 3, B6.FVB(Cg)-Tg(Drd1a-cre)FK150Gsat/Mmucd ; ID# 036916-UCD from MMRRC originally from GENSAT BAC Tg Project] and Drd2-Cre mice [n = 3, B6.FVB(Cg)-Tg(Drd2-cre)ER44Gsat/Mmucd ; ID# 032108-UCD from MMRRC originally from GENSAT BAC Tg Project] (~12 wks old) were

Author Manuscript Author Manuscript Author Manuscript Author Manuscript

group housed (2-4 subjects per cage) on a 12h:12h reverse light/dark cycle (lights off at 09.00 AM) throughout the duration of experiments with *ad libitum* access to food and water. Sample sizes were based on reports in related literature and were not predetermined by calculation.

Surgeries.—To label Drd1a- and Drd2-expressing mPFC neurons, AAV_5-EF1a-DIO-eYFP was injected bilaterally into the mPFC (AP: +1.8, ML: +0.3, DV: −2.75 & −2.4 [300 nl ea, bevel facing lateral]). Mice were allowed to recover and incubate for 4 wks. In a second surgery, 350 nl of Cholera Toxin subunit B (CTB) conjugated to Alexa Fluor-555, or 647 (Molecular Probes, Eugene, OR, USA) was injected into the dorsal periaqueductal gray (dPAG; AP: −4.2, ML: −0.5; DV: −2.4 mm) and NAc shell (AP: +1.0, ML: +0.75, DV: −4.5 mm) (in contralateral hemispheres, color counterbalanced) to retrogradely label mPFC-dPAG and mPFC-NAc projectors. Mice were sacrificed 6 days later as previously described. Histological, imaging, and data analyses are the similar to those previously described.

In vivo electrophysiology.

Subjects.—Male DAT::IRES-Cre mice (~6-8 wks old) were group housed (2-4 subjects per cage) on a 12h:12h reverse light/dark cycle (lights off at 09.00 AM) throughout the duration of experiments. Two days after head-bar adhesion (~2 wks before recordings), cages were placed on food restriction (4 hrs access to standard chow / day) with *ad libitum* access to water throughout training and recording. Sample sizes were based on reports in related literature and were not predetermined by calculation.

Surgery.—To achieve projection-specific ChR2 expression for *in vivo* photoidentification of mPFC-dPAG projectors, a virus encoding Cre-dependent ChR2 (AAV_5-Ef1a-DIO-ChR2-eYFP) was injected into the mPFC (AP: +1.8, ML: +0.3, DV: −2.75 & −2.4 [300 nl ea, bevel facing lateral]) and retrogradely traveling canine adeno-associated (CAV) virus carrying Cre-recombinase (CAV2-Cre; Institut de Génétique Moléculaire de Montpellier, France) was injected into the dPAG (AP: −4.2, ML: +0.5, DV: −2.4 [350 nl]). For manipulation of DA terminals, DAT::IRES-Cre mice received 1 ul of AAV_8-hSyn-FLEX-ChrimsonR-tdT in the VTA (AP: −3.4, ML: +0.4, DV: −4.25).

Head-bar adhesion.—After 11+ weeks of virus incubation, and ~2 weeks prior to behavioral training, mice were briefly anesthetized and a small aluminum head-bar (2 cm*2 mm*2 mm) was placed on the skull 5 mm posterior to the bregma along with one reference and one ground pin contacting the dura mater just anterior to the head-bar, in the contralateral cortex. A small pilot hole was made with a cranial drill above the mPFC and was marked with a pen. The area surrounding the pilot hole/mark was covered with petroleum jelly to prevent covering with dental cement. The three elements (head-bar, ground pin and reference pin) were cemented using one layer of adhesive cement (C&B metabond; Parkell, Edgewood, NY) followed by a layer of cranioplastic cement (Dental cement; Stoelting, Wood Dale, IL). After the cement dried, the pilot hole/mark was covered with a silicone gel (Kwik-Sil Adhesive, WPI, Sarasota, FL) to keep the bone clear during behavioral training.

Author Manuscript Author Manuscript Author Manuscript Author Manuscript

Behavior.—2 days after head-bar adhesion, mice were food restricted and pre-exposed to a 30% sucrose solution. Mice were head-fixed[59] in front of two small tubes one located just under the nose and the other above it pointed at the nose. The bottom tube delivered sucrose (training and recording days) and the top tube delivered airpuff (recording days only). Mice we trained to retrieve small drops (3 μL) of sucrose delivered through the bottom tube via a solenoid valve (Parker, Cleveland, OH), measured by breaks of an infrared beam recorded by an Arduino board (SmartProjects, Italy). Training sessions gradually increased in total duration (0.5 – 1.5 hr) and sucrose ITIs increased (15 – 80±8 s) over 5-8 days. The solenoid valves were triggered with a custom software written in LabVIEW (National instruments, Austin, TX) powered by NIDAQ-6251 and Arduino hardware.

Pre-recording craniotomy.—After 5-8 days of habituation and training, mice were briefly anesthetized with isoflurane (5% for induction, 1.5% after) and placed in a stereotaxic frame while their body temperature was controlled with a heating pad. A craniotomy was performed over the mPFC using the pilot hole/mark previously implemented using a hand-held drill. When the craniotomy was open, the dura was removed, blood cleaned with perfusion of saline, and then covered with petroleum jelly. Mice were removed from the stereotaxic and placed in a clean cage while their body temperature was maintained using a heat lamp until fully they recovered from anesthesia.

In vivo electrophysiological recordings and phototagging.—Once the mice recovered from the craniotomy surgery (at least 1 hr), they were head-fixed and a silicon optrode (A1×16-Poly2-5mm-50s- 177, NeuroNexus, Ann Arbor, MI) coated with red fluorescent latex microspheres (Lumafluor Inc.) was inserted into the anterior mPFC and lowered from the surface of the cortex for 1 mm at 10 μm/s using a motorized actuator (Z825B - 25 mm Motorized Actuator, Thorlabs, Newton, NJ, USA) mounted on a shuttle (460A linear stage, Newport, Irvine CA, USA) fixed to the stereotaxic arm. Next, the optrode was lowered for 1 mm at 1-2 μm/s. During the insertion of the electrode, sucrose was delivered every 60±8 s. After the probe was lowered to −2 mm below brain surface, sucrose deliveries were halted and a 10 min wait period commenced to let the tissue stabilize around the recording probe. Recording sessions were initiated using a RZ5D TDT system (Tucker-Davis Technologies, Alachua, FL, USA) while presenting ~ 40 sucrose and 40 airpuff trials (11 +/− 5 s ITI) randomly intermixed throughout the entire 30 min recording period. The recording period was broken into three 10 min epochs: 10 min into the recording period (first OFF epoch), 593 nm laser light pulse trains (20 Hz, 60 p, 5 ms pulses) were delivered through the optrode every 30 s for 10 min (20 pulse trains total, ON epoch). 10 more minutes were recorded in the absence of laser manipulation (second OFF epoch) – resulting in an OFF-ON-OFF epoch structure, with laser delivery only occurring during the ON epoch. Following completion of 30 min recording session, a photoidentification session using a 473 and/or 405 nm laser was conducted, during which pseudorandomly dispersed stimulations were delivered: 1 s constant light, 10× 1 Hz, 5 ms pulse trains, and 100 ms of 100 Hz (5 ms pulses). Recordings were then terminated and the optorde was lowered 300 um to a new recording site at 1-2 μm/s. The recording protocol was then repeated after a 30 min inter-session interval. Recordings sessions continued until we reached the bottom of the mPFC (−3 mm from brain surface) or when mice became sated and stopped retrieving

Author Manuscript Author Manuscript Author Manuscript Author Manuscript

sucrose. The electrode was then retracted at 5 μm/s, the craniotomy cleaned with saline, and covered with silicone gel (Kwik-Sil Adhesive, WPI, Sarasota, FL) to protect the brain until the next day of recording. During the second day of recording, the same procedure was repeated in a more posterior recording location. Following completion of the second day of recordings, mice were anesthetized with sodium pentobarbital and transcardially perfused. The brain was extracted, sectioned, and examined under a confocal microscope to verify the viral expression and the locations of the recording electrode.

Analysis of in vivo electrophysiological recordings.—Recording sessions were exported from the TDT format to Plexon offline sorter using OpenBridge (Tucker-Davis Technologies, Alachua, FL, USA). Offline sorter (Plexon, Dallas, TX, USA) was used to sort single units. Neural responses to sucrose / airpuff delivery and light stimulation were visualized through peristimulus time histograms (PSTH) and rasters for every unit using NeuroExplorer.

Data from Plexon and Neuroexplorer data files was then imported into MATLAB and analyzed using software written by P.N. Sucrose and airpuff PSTHs for each epoch (OFF-ON-OFF) were z-transformed using the histogram values in a 2 s baseline period starting 3 s prior to the onset of the stimulus. Similarly, PSTHs around a light pulse (used for photo identification of dPAG projectors) were z-transformed using a baseline window of 40 ms prior to the onset of the light pulse. To test significance of neural responses, Wilcoxon signed-rank tests were performed on the neural activity of each unit by comparing the number of spikes in a baseline window and an experimental window starting at the onset of stimulus or light pulse. The experimental window for AUC stimulus response was set to 0.5 s. The experimental window for light response was 8 ms based on the results of the *ex vivo* recordings. Significance threshold for the Wilcoxon signed-rank test was set at $p < 0.01$. Latency to the light pulse was defined as the first bin in the PSTH to cross 4 standard deviations relative to the 40 ms baseline window. Only units which met both criterion were considered phototagged and thus mPFC-dPAG projectors. Burst analyses were performed in NeuroExplorer using interval specifications. Bursts defined as three or more consecutive spikes with an interval of less than 25 ms in between the first two spikes and less than 50 ms in subsequent spikes, as previously defined for the mPFC[60].

Histology.

Perfusion and storage.—Subjects were deeply anesthetized with sodium pentobarbital (200 mg/kg; i.p.) and transcardially perfused with 15 mL (mouse) / 60 mL (rat) of Ringers solution followed by 15 mL (mouse) / 60 mL (rat) of cold 4% paraformaldehyde (PFA) dissolved in 1x PBS. Animals were decapitated and the brain was extracted from the cranial cavity and placed in 4% PFA solution and stored at 4 °C for at least 48 hrs. 36 hrs before tissue sectioning, brains were transferred to 30% sucrose solution dissolved in 1x PBS at room temperature. Upon sinking, brains were sectioned at 60 um on a freezing sliding microtome (HM420; Thermo Fischer Scientific). Sections were stored in 1x PBS at 4 °C until immunohistochemical processing.

Author Manuscript Author Manuscript Author Manuscript Author Manuscript

Immunohistochemistry.—Sections were blocked in 1x PBS - 0.3% Triton containing 3% donkey serum (Jackson ImmunoResearch, West Grove, USA), for 1 h at room temperature followed by incubation in primary antibody solution: chicken anti-TH (1:1000; Millipore, USA) or rabbit anti c-Fos (1:500; Santa Cruz Biotechnology, Dallas, TX, USA) in 1x PBS - 0.1% Triton containing 3% donkey serum for 48 h at 4 °C. Sections were then washed 4 times (10 min each) with 1x PBS and immediately transferred to secondary antibody solution: AlexaFluor 647-conjugated donkey anti-chicken (1:1000; Jackson ImmunoResearch, West Grove PA, USA) or Cy3 donkey anti-rabbit (1:500, Jackson ImmunoResearch, West Grove, PA, USA) and containing a DNA-specific fluorescent probe (DAPI; 1:50,000) in 1x PBS containing 3% donkey serum for 2 h at room temperature. Sections not processed for immunohistochemistry were incubated in 1x PBS - 0.3% Triton containing 3% normal donkey serum (Jackson ImmunoResearch, West Grove, USA) and DAPI (1:50,000) for 1 hr. Sections were washed 4 times (10 min each) in 1x PBS and mounted onto glass slides. Slices were allowed to dry and were coverslipped using polyvinyl alcohol (PVA) mounting medium with DABCO (Sigma, MO, USA). Stereotaxic coordinates were determined using brain atlases for rat[61] and mouse[62].

Confocal microscopy.—Fluorescent images were captured using a confocal laser scanning microscope (Olympus FV1000), with FluoView software (Olympus, Center Valley, PA), under a dry 10x / 0.40 NA objective, a 60x/1.42 NA oil immersion objective, or a 40x / 1.30 NA oil immersion objective. The locations of opsin expression, injection site, lesion from the optic fiber placement, and the position of carbon-fiber recording electrodes were determined by taking serial z-stack images through the 10x objective across a depth of 20-40 μm, with an optical slice thickness of 5-8 μm. High magnification images fluorescence quantifications were obtained through the 40x or 60x objective using serial z-stack images with an optical slice thickness of 3-4 μm (5 slices) using matched parameters and imaging locations. Fluorescence (in arbitrary units) was obtained from analysis in FIJI ImageJ. For quantitation of fluorescence across layers in the mPFC, measurements were normalized to the Z-stack containing the maximum value.

Sholl analysis.—Neurobiotin-filled/streptavidin stained mPFC-dPAG and mPFC-NAc projectors from *ex vivo* electorphysiology experiments were imaged at 40 x (1.30 NA oil immersion objective) using a confocal laser scanning microscope (Olympus FV100) covering the whole dendritic and axonal arborization in the slice. Neurons were reconstructed and Sholl analysis (# of intersections, 20 um rings from soma) performed using the “Simple Neurite Tracer” plugin contained in FIJI ImageJ (http://snyderlab.com/2016/05/25/tracing-neurons-using-fiji-imagej/).

Statistics.

Statistical analyses were performed using GraphPad Prism (GraphPad Software, Inc, La Jolla, CA) and MATLAB (Mathworks, Natick, MA). Group comparisons were made using one-way or two-way ANOVAs followed by Bonferroni post-hoc tests to control for multiple comparisons. Paired and unpaired two-way Student’s t-tests were used to make single-variable comparisons. Unpaired one-way t-tests were used to make comparisons with a priori hypotheses (time spent digging in marble burying assay). Tests for binomial

Author Manuscript Author Manuscript Author Manuscript Author Manuscript

distribution were also used on single populations. Non-parametric Wilcoxon signed rank tests were used to make comparisons between non-parametric data. Chi square tests were used to compare distribution of responsive cells between mPFC-dPAG and mPFC-NAc. All statistical tests were two-tailed unless otherwise noted as an *a priori* hypothesis. Thresholds for significance were placed at *p < 0.05, **p < 0.01, ***p < 0.001. All data are shown as mean ± standard error of the mean (SEM).

Data and code availability.

Data, unprocessed / unpsuedocolored images, and custom analysis codes are available upon request.

Extended Data

Author Manuscript Author Manuscript Author Manuscript Author Manuscript

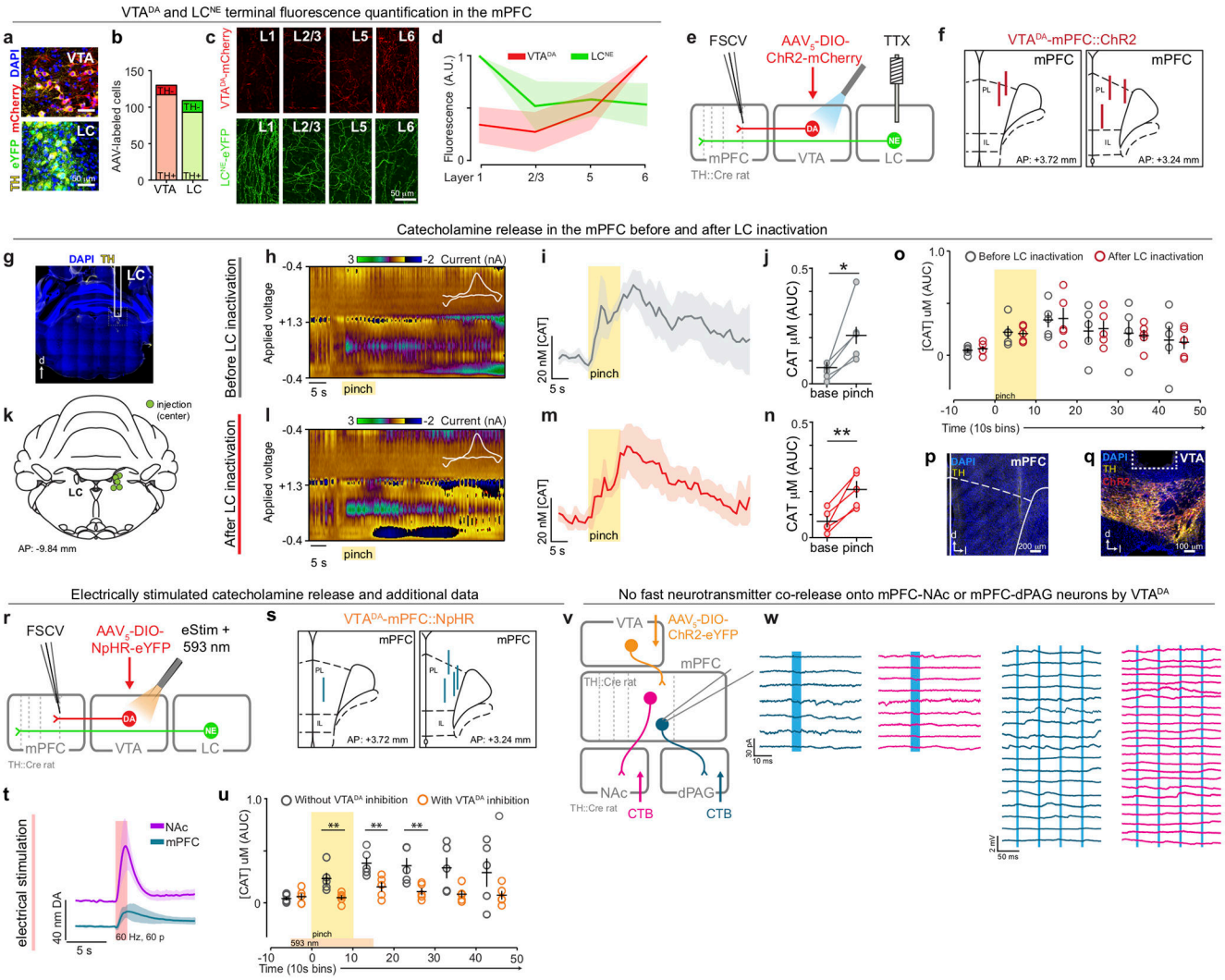

Extended Data Figure 1. Investigation of catecholamine terminal density and DA release dynamics in the mPFC.

(a) Injection of viral constructs enabling Cre-dependent expression into the LC and VTA of TH::Cre mice resulted in **(b)** fluorescent labeling of TH positive (TH+) noradrenergic (NE) neurons in the LC and DA neurons in the VTA. **(c)** Examination of VTA^{DA} and LC^{NE} fluorescent terminal labeling in the mPFC revealed different patterns of innervation by VTA^{DA} and LC^{NE} neurons across cortical layers in the prelimbic subregion of the mPFC (n = 3 mice). **(d)** VTA^{DA} terminals were densest in the deep (5 and 6) layers of the mPFC, while LC^{NE} terminals were denser in superficial (1 and 2/3) layers. **(e)** Schematic of strategy for differentiating dopamine and NE neurotransmission in the mPFC using fast-scan cyclic voltammetry (FSCV). VTA^{DA} neurons were selectively transduced with ChR2 in TH::Cre rats. After incubation, rats were prepared for anesthetized FSCV recordings where an optical fiber was implanted over the VTA and a guide cannula was positioned over the LC for tetrodotoxin (TTX)-mediated pharmacological inhibition. **(f)** A glass-encased carbon-fiber recording electrode was lowered into the mPFC for FSCV neurochemical measurements. Schematic representation of all recording electrode locations for ChR2 FSCV experiments.

Author Manuscript Author Manuscript Author Manuscript Author Manuscript

(g) Representative image of guide cannula track positioned over LC^{NE} cell bodies (yellow = TH). **h-j,** When VTA^{DA} and LC^{NE} neurons were intact, tail pinch (10 s in duration) rapidly increased extracellular catecholamine concentration ([CAT]), as shown in **(h)** a representative false color plot, **(i)** average CAT trace, and **(j)** concentration quantification (n = 5 rats) (two-tailed paired t-test, $t(4) = 3.402$, *p = 0.027). Color plot insets: representative cyclic voltammograms. **(k)** TTX + fast-green injection locations. **l-n,** After LC inactivation via intra-LC infusion of TTX, tail pinch evoked responses were maintained (two-tailed paired t-test, $t(4) = 5.249$, **p = 0.006). **(o)** Pharmacological inactivation of the LC with TTX did not significantly alter tail pinch evoked catecholamine release in the mPFC (two-way repeated measures ANOVA, $F_{5,40} = 0.061$, p = 0.997). **(p)** Representative image of FSCV electrode track in the mPFC. **(q)** Representative confocal image of ChR2-mCherry expression (red) in VTA^{DA} cell bodies (yellow = TH immunostaining). **(r)** Schematic of strategy to verify dependence of pinch-evoked increases in CAT neurotransmission on VTA^{DA} neurons. **(s)** Histologically verified FSCV recording electrode locations for NpHR experiments. **(t)** Electrical stimulation (60 Hz, 60 pulses, 200 uA) of the dorsal VTA evoked distinct patterns of dopamine release in the NAc and mPFC (n = 5 rats). **(u)** Optical inhibition (20 s constant 593 nm, 5mW) of NpHR-expressing VTA^{DA} neurons attenuated tail pinch evoked CAT release in the mPFC (two-way repeated measures ANOVA, $F_{5,40} = 2.857$, p = 0.027; Bonferroni post-hoc tests, **p < 0.01). **(v)** Schematic of viral strategy to optically manipulate ChR2-expressing VTA^{DA} terminals in the mPFC and record from dPAG- and NAc-projectors retrogradely labeled with cholera toxin (CTB) with *ex vivo* electrophysiology. **(w)** No evidence of co-release of fast-synaptic neurotransmitters (i.e., glutamate and GABA) from VTA^{DA} terminals onto either mPFC-dPAG (teal) or mPFC-NAc (pink) populations following optical stimulation in voltage-clamp (left) and current-clamp (right). Error bars and shading represent ±SEM. A.U. = arbitrary fluorescence units. AUC = area under the curve. The rat brain in this figure was reproduced with permission from Paxinos and Watson, 2006.

Author Manuscript Author Manuscript Author Manuscript Author Manuscript

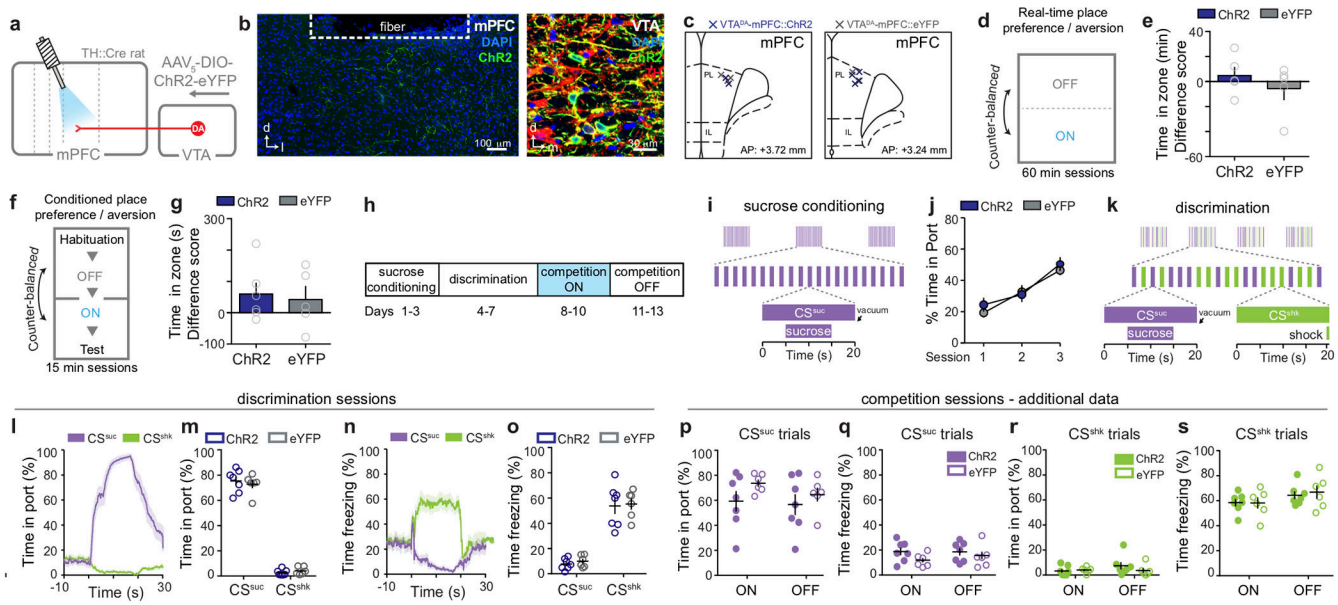

Extended Data Figure 2. Activation of VTA^{DA} terminals in the mPFC does not support real-time or conditioned place preference.

(a) Schematic of strategy for manipulating dopamine release in the mPFC. VTA^{DA} neurons were selectively transduced with ChR2 in TH::Cre rats and guide cannulae were implanted over the mPFC for the insertion of an optical fiber for light delivery. **(b)** Representative confocal image of ChR2-eYFP expression in VTA^{DA}-mPFC underneath a guide cannula (left) and expression in the VTA (right). **(c)** Histological verification of guide cannulae placements in the mPFC for ChR2 subjects (left) and eYFP controls (right). **(d)** Schematic of experimental design RTPP/A. When rats entered the ON zone, laser light stimulation was activated for the duration of the time spent in the ON zone (20 Hz, 60 p, every 30 s, 20 mW of 473 nm for VTA^{DA}-mPFC experiments). When rats entered the OFF zone, light stimulation was terminated for the duration of time spent in the OFF zone. **(e)** Optogenetic stimulation of VTA^{DA} neurons did not evoke real-time place avoidance or preference in VTA^{DA}-mPFC::ChR2 animals (n = 5), compared to VTA^{DA}-mPFC::eYFP controls (n = 5), measured by difference score [minutes spent in the ON zone – OFF zone] (two-tailed unpaired t-test, t(8) = 0.9337, p = 0.3778). **(f)** Schematic of experimental design for CPP/A. Day 1 consisted of a habituation period where time spent on each compartment of the arena was recorded. On days 2 and 3, a divider was placed in the middle of the chamber to separate the two compartments and rats received either no stimulation (OFF) or stimulation (ON) (20 Hz, 60 p, every 30 s, 20 mW of 473 nm light for VTA^{DA}-mPFC experiments), counter-balanced across days. On day 4, the divider was removed and time spent in each compartment was recorded in the absence of stimulation (i.e., test day). **(g)** Optogenetic stimulation of VTA^{DA} neurons did not support conditioned place aversion or preference in VTA^{DA}-mPFC::ChR2 animals (n = 6), compared to VTA^{DA}-mPFC::eYFP controls (n = 5), measured by difference score [minutes spent in the ON zone – OFF zone] (two-tailed unpaired t-test, t(9) = 0.3192, p = 0.7569). **(h)** Schematic of task used to examine dopamine modulation of reward and fear-motivated behaviors during competition. **(i)** During sucrose training, a CS (light or tone, counterbalanced) predicted sucrose delivery (CS^{suc}). Sucrose

Author Manuscript Author Manuscript Author Manuscript Author Manuscript

was removed from the delivery port by vacuum if not collected. **(j)** VTA^{DA}-mPFC::ChR2 rats (n = 7) and VTA^{DA}-mPFC::eYFP controls (n =6) acquired sucrose conditioning similarly (two-way repeated measures ANOVA, $F_{2,22} = 0.7$, p = 0.5090). **(k)** During discrimination, the alternative CS (light or tone, counterbalanced) was introduced and predicted foot shock (CS^{shk}). **(l)** Average traces showing time spent in the sucrose port before, during, and after each CS presentation (grouped, n = 13 rats). **(m)** Time spent in the sucrose port did not differ between VTA^{DA}-mPFC::ChR2 rats (n = 7) and VTA^{DA}-mPFC::eYFP controls (n = 6) during CS^{suc} or CS^{shk} presentation (repeated measures two-way ANOVA, $F_{1,11} = 0.54$, p = 0.4789). **(n)** Average traces showing time spent freezing before, during, and after each CS presentation (grouped, n = 13 rats). **(o)** Time spent freezing did not differ between VTA^{DA}-mPFC::ChR2 rats and VTA^{DA}-mPFC::eYFP controls during CS^{suc} or CS^{shk} (repeated measures two-way ANOVA, $F_{1,11} = 0.01$, p = 0.9281) presentation. **(p)** During competition sessions, the average time spent in the reward port for CS^{suc} trials during ON sessions and CS^{suc} trials during OFF sessions did not differ between ChR2 rats (n = 7, closed bars) and eYFP controls (n = 6, open bars) (repeated measures two-way ANOVA, $F_{1,11} = 0.82$, p = 0.3845). Note that during ON sessions, stimulation was only delivered during the CS^{comp} trials. **(q)** Average time spent freezing for CS^{suc} trials during ON sessions and CS^{suc} trials during OFF sessions did not differ between ChR2 rats (closed bars) and eYFP controls (repeated measures two-way ANOVA, $F_{1,11} = 1.35$, p = 0.2705). **(r)** During competition sessions, the average time spent in the reward port for CS^{shk} trials during ON sessions and CS^{shk} trials during OFF sessions was not different between ChR2 (closed bars) and eYFP controls (open bars, repeated measures two-way ANOVA, $F_{1,11} = 0.94$, p = 0.354). **(s)** During competition sessions, the average time spent freezing for CS^{shk} trials during ON sessions and CS^{shk} trials during OFF sessions was not different between ChR2 rats (closed bars) and eYFP controls (open bars, repeated measures two-way ANOVA, $F_{1,11} = 0.16$, p = 0.6998). Error bars and shading represent ±SEM.

Author Manuscript Author Manuscript Author Manuscript Author Manuscript

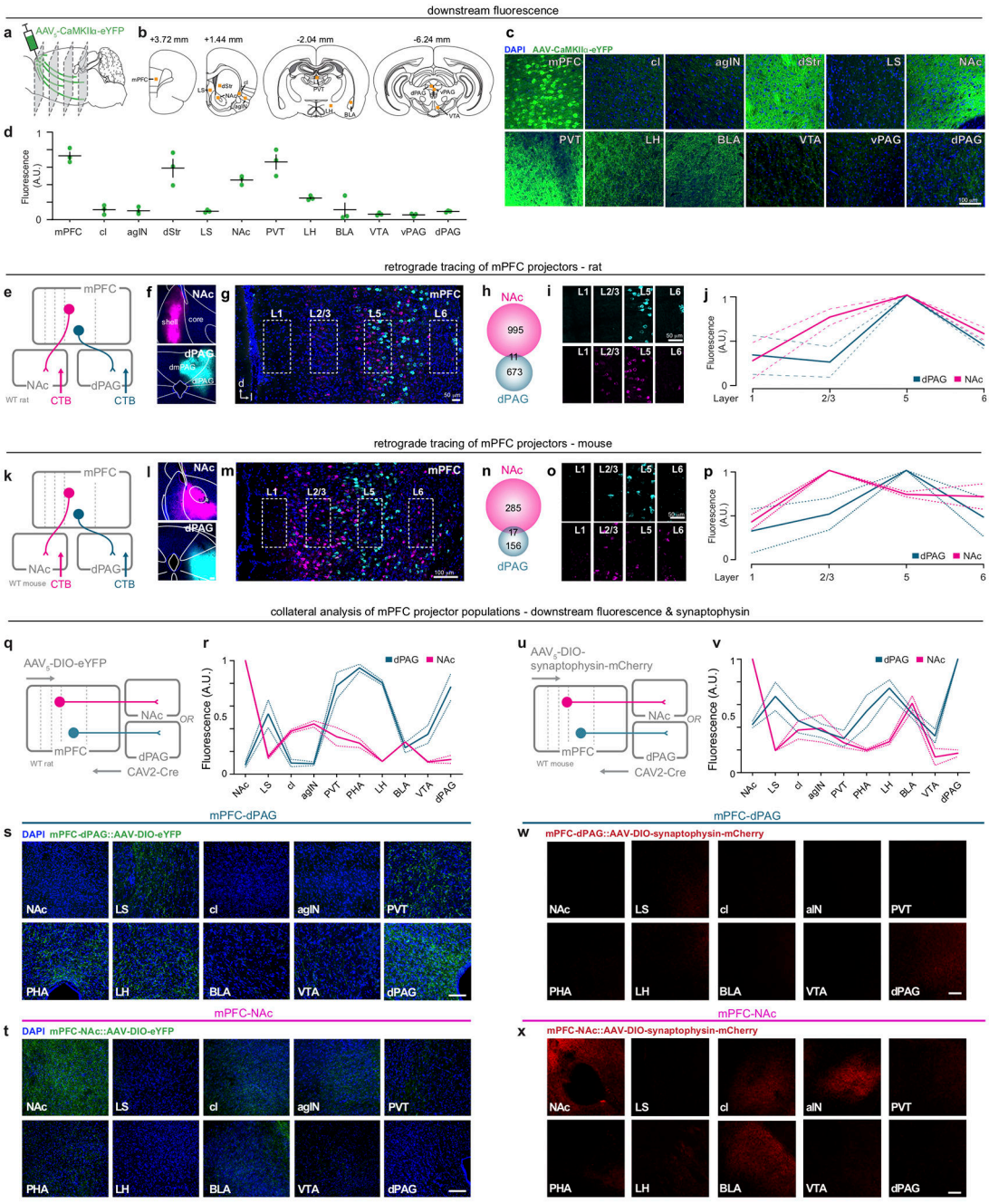

Extended Data Figure 3. Putative connection strength of mPFC projections to downstream targets, layer localization of projectors, and collateralization.

(a) Schematic of strategy where anterogradely traveling virus was injected into the prelimbic and infralimbic subregions of the mPFC and fluorescence was quantified in several downstream brain regions. **(b)** Orange boxes represent approximate locations of fluorescence quantification, as a proxy for connection strength (n = 3 rats). **(c)** Representative images and **(d)** quantification of fluorescence in the mPFC and downstream targets in the rat. **(e)** Microinjections of cholera toxin subunit B (CTB) conjugated to

Author Manuscript Author Manuscript Author Manuscript Author Manuscript

fluorescent proteins (AlexaFluor-488, −555, or −647, counter-balanced) were placed in the dPAG and NAc to retrogradely label the cell bodies of projection neurons in the rat mPFC (n = 3 rats). **(f)** Representative confocal images of CTB injections in the NAc and dPAG of the rat. **(g)** Representative confocal image of retrogradely labeled neurons in the rat mPFC. **(h)** As a population, only 11 out of 1,679 CTB+ neurons in the mPFC were dual-labeled. **(i)** Fluorescence quantification of retrogradely labeled mPFC-dPAG and mPFC-NAc neurons revealed differences in cell body location across cortical layers in the rat mPFC. **(j)** In the rat, dPAG-projectors predominantly originate from deep layer 5, whereas NAc-projectors are located in both superficial layers 2/3 and deep layer 5. **(k)** Microinjections of CTB conjugated to fluorescent proteins were placed in the dPAG and NAc to retrogradely label the cell bodies of projection neurons in the mouse mPFC. **(l)** Representative confocal images of CTB injections in the NAc and dPAG of the mouse (n = 3 mice). **(m)** Representative confocal image of retrogradely labeled neurons in the mouse mPFC. **(n)** As a population, only 17 out of 458 CTB+ neurons in the mPFC were dual-labeled. **(o)** Fluorescence quantification of retrogradely labeled mPFC-dPAG and mPFC-NAc neurons revealed differences in cell body location across cortical layers in the mouse mPFC. **(p)** In the mouse, dPAG-projectors predominantly originate from deep layer 5, whereas NAc-projectors are located in both superficial layers 2/3 and deep layer 5.**(q)** Schematic of viral strategy to explore downstream fluorescence from mPFC-NAc::eYFP (n = 3 rats) and mPFC-dPAG::eYFP (n = 3 rats) projectors. **(r)** Quantification of fluorescence in the mPFC and downstream brain regions originating from mPFC-dPAG::eYFP and mPFC-NAc::eYFP neurons. **(s)** Representative confocal images from a mPFC-dPAG::eYFP subject and **(t)** mPFC-NAc::eYFP subject. **(u)** Schematic of viral strategy to explore downstream terminals from mPFC-NAc::synaptophysin (n = 3 mice) and mPFC-dPAG::synaptophysin (n = 3 mice) projectors. **(v)** Quantification of fluorescence in the mPFC and downstream brain regions originating from mPFC-dPAG::synaptophysin and mPFC-NAc::synaptophysin neurons. **(w)** Representative confocal images from a mPFC-dPAG::synaptophysin subject and **(x)** mPFC-NAc::synaptophysin subject. Abbreviations: agIN = agranular insula; BLA = basolateral amygdala; cl = claustrum dPAG = dorsal periaqueductal gray; dStr = dorsal striatum (medial); LH = lateral hypothalamus; LS = lateral septum; mPFC = medial prefrontal cortex; NAc = nucleus accumbens; PHA = posterior hypothalamic area; PVT = paraventricular nucleus of the thalamus; vPAG = ventral periaqueductal gray; VTA = ventral tegmental area. Rat and mouse brains in this figure has been reproduced with permission from Paxinos and Watson, 2006 and Paxinos and Franklin, 2004, respectively. Error bars and dashed lines represent ±SEM.

Author Manuscript Author Manuscript Author Manuscript Author Manuscript

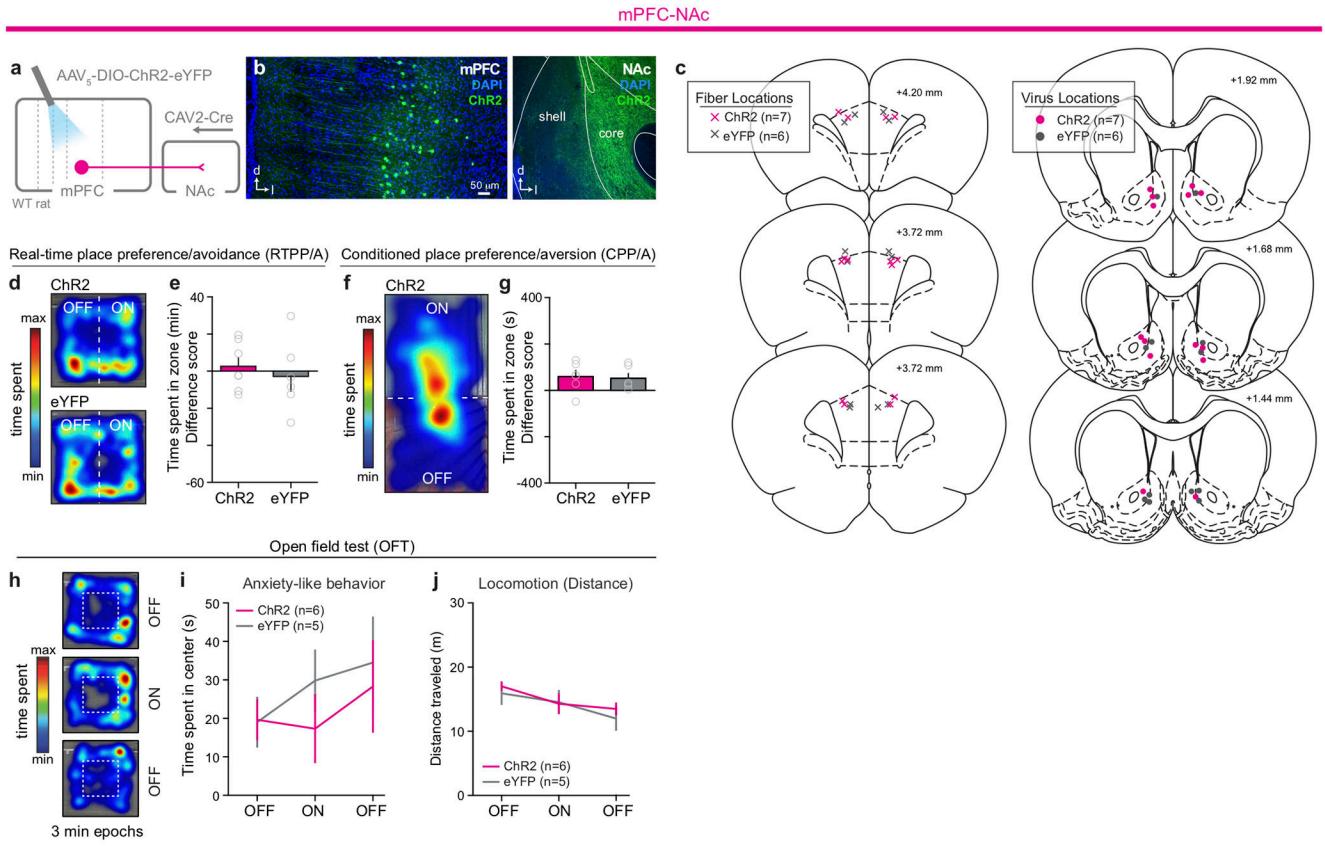

Extended Data Figure 4. mPFC-NAc photostimulation does not support place preference or aversion.

(a) Schematic of viral transduction strategy to achieve optogenetic control of rat mPFC neurons projecting to the NAc. **(b)** Representative image of NAc-projecting mPFC neurons expressing ChR2 (left) and ChR2+ terminals in the NAc. **(c)** Histological verification of bilateral optical fiber implant locations above the mPFC and virus injection locations in the NAc. **(d)** Representative locomotor heatmaps of mPFC-NAc::ChR2 (top) and mPFC-NAc::eYFP (bottom) subjects in RTPP/A. **(e)** Optogenetic stimulation of mPFC-NAc neurons did not evoke real-time place avoidance or preference in mPFC-NAc::ChR2 animals (n = 7 rats), compared to mPFC-NAc::eYFP controls (n = 6 rats), measured by difference score [minutes spent in the ON zone – OFF zone] (two-tailed unpaired t-test, t(11) = 0.5549, p = 0.5901). **(f)** Representative locomotor heatmap of mPFC-NAc::ChR2 subject in CPP/A assay. **(g)** Optogenetic stimulation of mPFC-NAc neurons did not evoke real-time place aversion or preference in mPFC-NAc::ChR2 animals (n = 6 rats), compared to mPFC-NAc::eYFP controls (n = 6 rats), measured by difference score [minutes spent in the ON zone – OFF zone] (two-tailed unpaired t-test, t(10) = 0.2143, p = 0.8346).**(h)** Representative locomotor heatmaps of a mPFC-NAc::ChR2 subject during 3 min OFF-ON-OFF epochs during the open-field test (OFT). **(i)** Optical activation of mPFC-NAc::ChR2 (n = 6 rats) did not change time spent in the center region compared to eYFP controls (n = 5 rats), as measured by time spent in the center of the arena (two-way repeated measures ANOVA, $F_{2,18} = 0.74$, p = 0.4913), or **(j)** general locomotor activity (two-way rep eated measures

Author Manuscript Author Manuscript Author Manuscript Author Manuscript

ANOVA, $F_{2,18} = 0.61$, $p = 0.5532$). Error bars indicate ±SEM. The rat brains in this figure were reproduced with permission from Paxinos and Watson, 2006.

Author Manuscript Author Manuscript Author Manuscript Author Manuscript

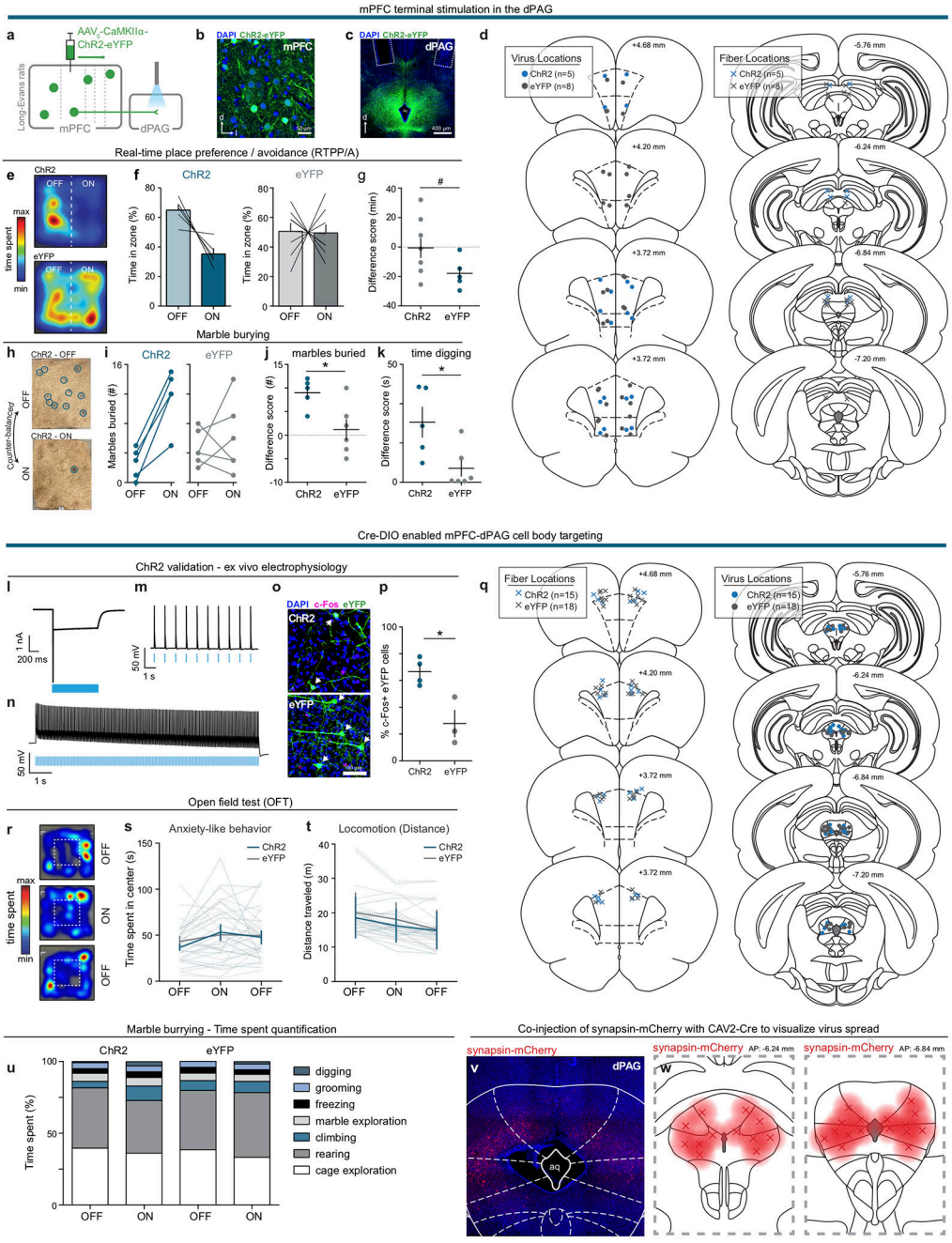

Extended Data Figure 5. Activation of mPFC terminals in the dPAG increase marble burying and activation of mPFC-dPAG cell bodies does not affect anxiety-like behavior.

(a) Schematic of viral strategy to achieve optogenetic control of ChR2-expressing mPFC terminals in the dPAG. **(b)** Representative image of ChR2+ neurons in the mPFC and (**c**) ChR2+ terminals in the dPAG (optic fiber lesions indicated by dashed lines). **(d)** Histological verification of bilateral virus injection locations in the mPFC and bilateral optic fiber implant locations above the dPAG. **(e)** Representative locomotor heatmaps of mPFC-dPAG::ChR2 (top) compared to mPFC-dPAG::eYFP control subject (bottom) in RTPP/A

Author Manuscript Author Manuscript Author Manuscript Author Manuscript

assay. **(f)** Percent of time spent in the ON and OFF zones of the arena in mPFC-dPAG::ChR2 and mPFC-dPAG::eYFP subjects. **(g)** Optogenetic stimulation of mPFC terminals in the dPAG resulted in a trend towards avoidance in the real-time place avoidance assay in mPFC-dPAG::ChR2 animals (n = 5 rats), compared with mPFC-dPAG::eYFP controls (n = 8 rats) (two-tailed unpaired t-test, t(11) = 1.830, #p = 0.0944). **(h)** Representative arena of mPFC-dPAG::ChR2 animal after marble burying assay when optical stimulation was OFF (top) and ON (bottom). **(i)** Number of marbles buried in mPFC-dPAG::ChR2 (n = 5 rats) and mPFC-dPAG::eYFP (n = 6 rats) during OFF and ON sessions. **(j)** Optical stimulation of mPFC-dPAG neurons resulted in more marbles buried by mPFC-dPAG::ChR2 animals, compared with mPFC-dPAG::eYFP controls (two-tailed unpaired t-test, t(9) = 2.839, *p = 0.0194) and **(k)** more time digging (one-tailed unpaired t-test, t(9) = 2.775, *p = 0.0108). **(l)** Functional ChR2 expression in mPFC-dPAG neurons was verified by targeted ex *vivo* whole-cell patch-clamp electrophysiology. Recording from a ChR2-expressing mPFC-dPAG neuron in voltage-clamp mode showing sustained inward current elicited by a 1 s pulse of 470 nm light. **(m)** In current-clamp mode, action potentials were elicited by 1 Hz and (**n**) 20 Hz light trains (470 nm, 5 ms pulse-duration. **(o)** Representative confocal images of mPFC-dPAG::ChR2 (top) and mPFC-dPAG::eYFP expressing neurons showing immediate early gene (c-Fos) expression following 5 min of blue (473 nm) light exposure (20 Hz, 5 ms pulse-duration, 15 mW). **(p)** 473 nm laser light stimulation enhanced the number of immediate early gene (c-Fos) positive ChR2-expressing mPFC-dPAG neurons compared with control mPFC-dPAG::eYFP neurons (mPFC-dPAG::ChR2 n = 4 rats; mPFC-dPAG::eYFP n = 3 rats; two-tailed unpaired t-test, t(5) = 3.707, *p = 0.014). **(q)** Histological verification of bilateral optical fiber implant locations above the mPFC and virus injection locations in the dPAG for remaining mPFC-dPAG::ChR2/eYFP expressing rats. **(r)** Representative locomotor heatmaps of a mPFC-dPAG::ChR2 subject during 3 min OFF-ON-OFF epochs in the open-field test (OFT). **(s)** Optical activation of mPFC-dPAG::ChR2 (n = 15 rats) did not change time spent in the center region compared to eYFP controls (n = 18 rats), as measured by time spent in the center of the arena (two-way repeated measures ANOVA, group x epoch, $F_{2,62} = 0.37$, p = 0.69), or **(t)** general locomotor activity (distance traveled, two-way repeated measures ANOVA, group x epoch interaction, $F_{2,62} = 0.9412$, p = 0.3957). **(u)** Quantification of behaviors (% time engaging) during marble burying assay. **(v)** Representative confocal image of viral spread in the PAG, visualized by co-injection of AAV_5-hSyn-mCherry (hSyn = synapsin, red) with CAV2-Cre in a subset of mPFC-dPAG::ChR2/eYFP expressing rats. **(w)** Illustration of reconstructed injection locations and spread in co-injected subjects (n = 14 total, 7 ChR2, 7 eYFP). Error bars indicate ±SEM. The rat brains in this figure were reproduced with permission from Paxinos and Watson, 2006.

Author Manuscript Author Manuscript Author Manuscript Author Manuscript

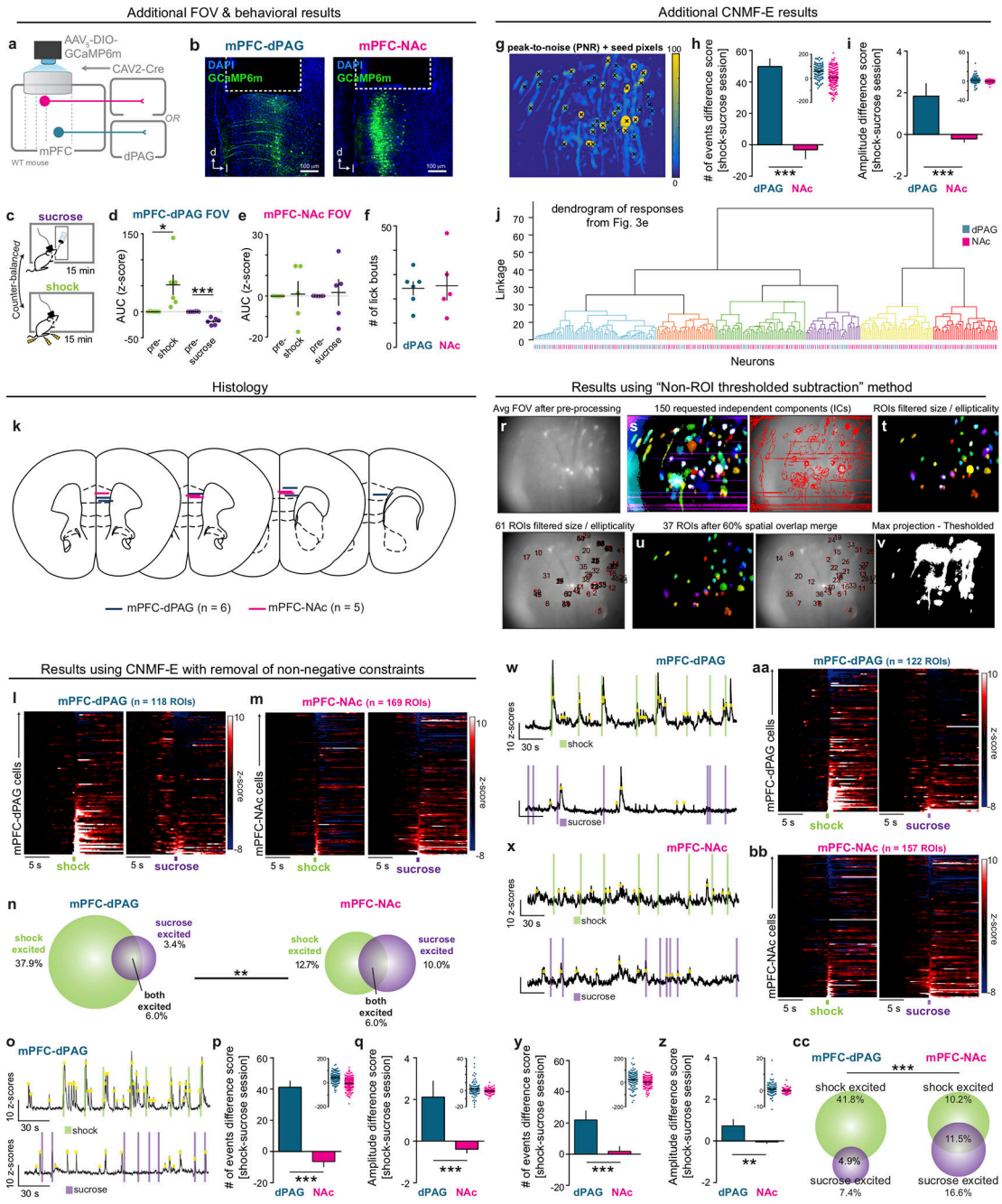

Extended Data Figure 6. Analysis and additional data from epifluorescent calcium imaging experiments during sucrose and shock delivery.

(a) Schematic of strategy for monitoring neuronal activity in mPFC-dPAG and mPFC-NAc neurons using *in vivo* calcium imaging. **(b)** Representative confocal images of mPFC-NAc::GCaMP6m (left) and mPFC-dPAG::GCaMP6m neurons (right) underneath GRIN lenses (dashed lines). **(c)** Dynamic calcium fluctuations were monitored during a 15 min recording session where mice were allowed to self-administer sucrose via a sucrose lickometer or had random, unsignaled foot shocks delivered. **(d)** As a population, mPFC-

Author Manuscript Author Manuscript Author Manuscript Author Manuscript

dPAG::GCaMP6m (n = 6 mice) were are activated to foot shock (green, two-tailed paired t-test, t(5)=2.616, *p = 0.0473) and inhibited by the initiation of a sucrose bout (purple, two-tailed paired t-test, t(5)=6.982, ***p = 0.0009) as measured by the bulk fluorescence across the entire field of view (FOV) (−3 – 0 s = pre-; 0 – 3 s = shock/sucrose). **(e)** As a population, mPFC-NAc::GCaMP6m (n = 5 mice) were not responsive to foot shock (green, two-tailed paired t-test, t(4)=0.1520, p = 0.8866) or the initiation of a sucrose bout (purple, two-tailed paired t-test, t(4)=0.2678, p = 0.8021) (−3 – 0 s = pre-; 0 – 3 s = shock/sucrose). **(f)** mPFC-dPAG::GCaMP6m and mPFC-NAc::GCaMP6m mice did not differ in the number of lick bouts initiated during the sucrose session (two-tailed unpaired t-test, t(9)=0.1666, p = 0.8714). **(g)** Peak-to-noise heatmap generated from a representative FOV with seed pixels overlaid (black X). **(h)** mPFC-dPAG::GCaMP6m neurons (n = 118 ROIs) had more frequent calcium transients than mPFC-NAc::GCaMP6m neurons (n = 169 ROIs) during the shock session (# of events difference score [shock-sucrose]), dPAG Mdn = 51.5, NAc Mdn = −6, two-tailed Mann Whitney test, U = 5840, ***p < 0.0001). **(i)** mPFC-dPAG::GCaMP6m neurons had higher amplitude transients than mPFC-NAc::GCaMP6m neurons during the shock session (amplitude of events difference score [shock-sucrose]), dPAG Mdn = 0.9031, NAc Mdn = −0.3549, Mann Whitney test, U = 6672, ***p < 0.0001). **(j)** Dendrogram of agglomerative hierarchical clustering. Different colors represent clusters based on average responses per ROI to footshock and sucrose. **(k)** Histologically verified locations of GRIN lens implants. **l-cc,** In addition to using CNMF-E, imaging data were analyzed using two other approaches: 1) a modified constrained CNMF-E algorithm considering calcium fluctuations can have negative transients, associated with a decrease in firing (Otis et al., 2017; Kaupferschmidt et al., 2017). For the approach, we did not constrain values to > 0. And 2) Data were also analyzed with 2) a ROI based method [i.e.,“non-ROI”, **r-cc**]. **(l)** Calcium signals were extracted from individual ROIs and the average calcium traces per ROI were aligned to shock and sucrose bout onset for mPFC-NAc::GCaMP6m and **(m)** mPFC-dPAG::GCaMP6m recordings. **(n)** The distribution of shock and sucrose excited cells for mPFC-dPAG::GCaMP6m neurons was different from mPFC-NAc::GCaMP6m neurons (chi square, $X^2 = 10.95$, **p = 0.0042). **(o)** Representative calcium traces from a mPFC-dPAG::GCaMP6m neuron during shock (top) and sucrose (bottom) recording sessions. Individual calcium transients (yellow dots) were identified and quantified. **(p)** mPFC-dPAG::GCaMP6m neurons (n = 118 ROIs) had more frequent calcium transients than mPFC-NAc::GCaMP6m neurons (n = 169 ROIs) during the shock session (# of events difference score [shock-sucrose]), dPAG Mdn = 43, NAc Mdn = −3, two-tailed Mann Whitney test, U = 4373, ***p < 0.0001). **(q)** mPFC-dPAG::GCaMP6m neurons had higher amplitude calcium transients compared to mPFC-NAc::GCaMP6m neurons during the shock session (amplitude of events difference score [shock-sucrose]), dPAG Mdn = 1.329, NAc Mdn = −0.2459, two-tailed Mann-Whitney test, U = 7164, ***p < 0.0001). **(r)** Mean Z-projection image of the entire FOV through the relay lens after image pre-processing. Recordings were converted to changes in fluorescence compared to background fluorescence (F-F0)/F0 using the mean Z-projection image as reference (F0). **(s)** Calcium signals arising from ROIs were identified using independent and principal component analyses (PCA/ICA). **(t)** Identified PCA/ICA filters were thresholded at their half-max values to define possible ROIs and were screened for neuronal morphology. ROIs were only accepted if the threshold filters included only on contiguous region with an eccentricity of

Author Manuscript Author Manuscript Author Manuscript Author Manuscript

<0.85 and an area between 30-350 pixels. In this example, 61 ROIs (of the original 150 ICs) met these criteria. **(u)** Accepted ROI filters were then merged if their areas overlapped by more than 60%. In this example, 24 ROIs were merged for a remaining total of 37 valid ROIs. **(v)** To acquire the non-ROI thresholded image for background subtraction, max Z-projections of individual recordings were created and thresholded to separate ROIs and their processes from the rest of the field of view. Average signal from the remaining pixels was used as a proxy for the whole field changes in fluorescence, and regressed of the signal from each ROI. **(w)** Calcium transients (yellow dots) within individual mPFC-dPAG::GCaMP6m neurons and **(x)** mPFC-NAc::GCaMP6m neurons were quantified (representative traces). **(y)** mPFC-dPAG::GCaMP6m neurons (n = 113 ROIs) had more frequent calcium transients than mPFC-NAc::GCaMP6m neurons (n = 157 ROIs) during the shock session (difference score [shock-sucrose], dPAG Mdn = 30, NAc Mdn = 6, two-tailed Mann Whitney test, U = 6392, ***p < 0.0001). **(z)** mPFC-dPAG::GCaMP6m neurons had larger amplitude calcium transients than mPFC-NAc::GCaMP6m neurons during the shock session (difference score [shock-sucrose], dPAG Mdn = 0.5158, NAc Mdn = −0.0615, two-tailed Mann-Whitney test, U = 7065, **p = 0.0044). **(aa)** Average calcium traces per cell for mPFC-dPAG::GCaMP6m neurons and **(bb)** mPFC-NAc::GCaMP6m neurons were aligned to shock (left) and sucrose bout (right). **(cc)** The distribution of shock and sucrose excited cells for mPFC-dPAG::GCaMP6m (n = 118 ROIs) neurons were different from mPFC-NAc::GCaMP6m neurons (n = 157 ROIs) (chi square, $X^2 = 32.33$, ***p < 0.0001). FOV = field of view. Error bars and + indicate ±SEM. Scale bar = 100 um. The mouse brains in this figure were reproduced with permission from Paxinos and Franklin, 2004.

Author Manuscript Author Manuscript Author Manuscript Author Manuscript

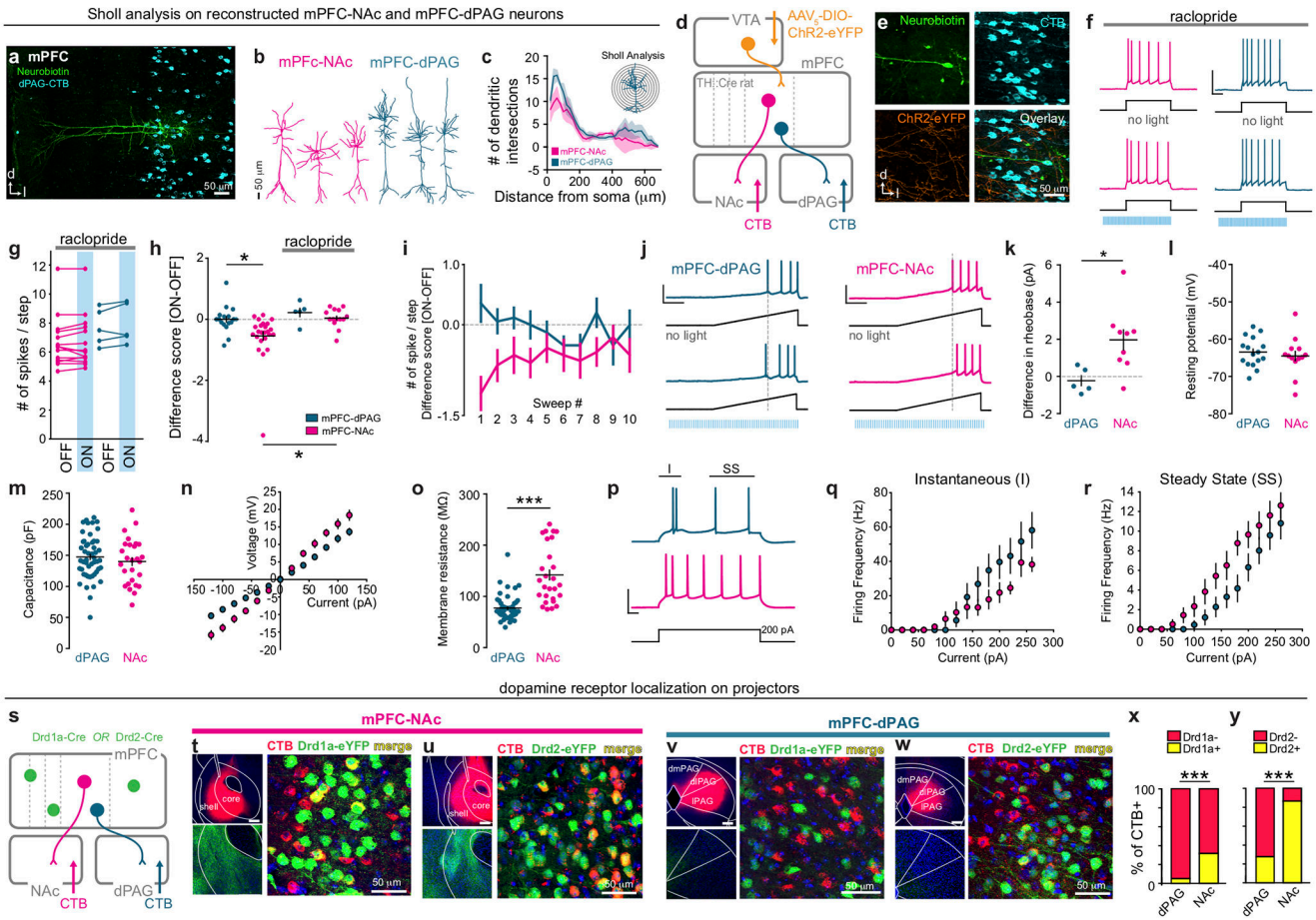

Extended Data Figure 7. VTA^{DA} effects on mPFC projectors across time and their properties.

(a) Representative confocal image of mPFC-dPAG labeled neurons. **(b)** Representative examples of reconstructed mPFC-NAc and mPFC-PAG neurons. **(c)** Sholl analysis of mPFC-NAc (n = 4 cells) and mPFC-dPAG (n = 4 cells) subpopulations. **(d)** Schematic of viral strategy to optically manipulate ChR2-expressing VTA^{DA} terminals in the mPFC and record from dPAG- and NAc-projectors retrogradely labeled with cholera toxin (CTB) using *ex vivo* electrophysiology. **(e)** Representative images of a recorded mPFC-dPAG neuron (neurobiotin+ and CTB+) surrounded by ChR2-eYFP+ VTA^{DA} terminals. **(f)** Representative traces of a mPFC-dPAG and mPFC-NAc neuron during a current step without (top) and with (bottom) optogenetic activation of VTA^{DA} terminals in the presence of D2-type dopamine receptor blockade via bath applied raclopride. **(g)** The change in spike number with optical stimulation (ON-OFF) recorded from mPFC-dPAG (n = 5 cells) and mPFC-NAc neurons (n = 14 cells) in the presence of D2-receptor antagonism. **(h)** The change in spike number with optical stimulation (ON-OFF) was different between mPFC-dPAG (n = 17 cells) and mPFC-NAc neurons (n = 24 cells) and was blocked by D2-receptor antagonism (one-way ANOVA, $F_{3,56} = 5.343$, p = 0.0026, Bonferroni multiple comparisons tests, dPAG vs. NAc *p = 0.0040, NAc vs. NAc + rac *p = 0.0034). **(i)** Change in the number of spikes per step with optical stimulation (ON-OFF) for individual sweeps. mPFC-NAc neurons exhibited a more robust decrease in spike number during VTA^{DA} terminal stimulation during the first few

Author Manuscript Author Manuscript Author Manuscript Author Manuscript

sweeps, an effect that diminished in later sweeps. **(j)** Representative traces showing firing elicited in mPFC-dPAG and mPFC-NAc neurons in response to current ramp with and without VTA^{DA} terminal stimulation (grey dashed line indicates time of first action potential without optical stimulation). **(k)** Optical stimulation of VTA^{DA} terminals increased the current required to elicit an action potential (rheobase) in NAc-projectors. The change in rheobase with optical stimulation (ON-OFF) was different between dPAG-projectors (n = 5 cells) and NAc-projectors (n = 9 cells) (two-tailed unpaired t-test, t(12) = 2.669, p = 0.0205). **(l)** Neither resting membrane potential (mPFC-dPAG n = 16 cells; mPFC-NAc n =13 cells) nor **(m)** capacitance differed between dPAG-projectors (n = 42 cells) and NAc-projectors (n = 27 cells) (resting membrane potential: two-tailed unpaired t-test, t(27) = 0.6265, p = 0.5363; capacitance: two-tailed unpaired t-test, t(75) = 0.8643, p = 0.3902). **(n)** The current-voltage (I-V) relationship of mPFC-dPAG (n = 16 cells) and mPFC-NAc (n = 13 cells) neurons obtained by applying a series of current steps in voltage-clamp mode (two-way ANOVA, $F_{12,24} = 10.16$, $p < 0.0001$). **(o)** The membrane resistance was significantly greater in NAc-projectors (n = 27 cells) compared to dPAG-projectors (n = 50 cells) (two-tailed unpaired t-test, t(75) = 7.030, ****p < 0.0001). **(p)** Representative traces showing action potential firing in mPFC-dPAG and mPFC-NAc neurons in response to a depolarizing current step. **(q)** Instantaneous (I) and **(r)** steady state (SS) firing frequency in dPAG- and NAc-projectors in response to increasing current steps. **(s)** Schematic of strategy for identifying dopamine receptor type 1 (D1) and dopamine receptor type 2 (D2) on mPFC-projector populations using transgenic mice (Drd1a-Cre [n = 3 mice] and Drd2-Cre [n = 3 mice]), retrograde labeling, and Cre-dependent eYFP recombination. **(t)** Representative confocal images of NAc CTB injections sites (upper left), mPFC terminal fluorescence (lower left), and mPFC-NAc cell bodies (right) in a Drd1a-Cre::eYFP mouse and **(u)** Drd2-Cre::eYFP mouse. **(v)** Representative confocal images of dPAG CTB injections sites (upper left), mPFC terminal fluorescence (lower left), and mPFC-dPAG cell bodies (right) in a Drd1a-Cre::eYFP mouse and **(w)** a Drd2-Cre::eYFP mouse. **(x)** 5% of mPFC-dPAG CTB+ neurons were Drd1a+ (19/378), whereas 31.5% of mPFC-NAc CTB+ neurons were co-labeled as Drd1a+ (15¼79) (D1 chi square, $X^2 = 93.29$, ***p < 0.0001). **(y)** 27.6% of mPFC-dPAG CTB+ neurons were Drd2+ (74/342), whereas 86.3% of mPFC-NAc CTB+ neurons were co-labeled as Drd2+ (414/480) (D2 chi square, $X^2 = 345.6$, ***p < 0.0001). Error bars, shading, and + represent ±SEM. Scale bars (histology) = 50 μm. Scale bars (electrophysiology) = 500 ms. 50 mV.

Author Manuscript Author Manuscript Author Manuscript Author Manuscript

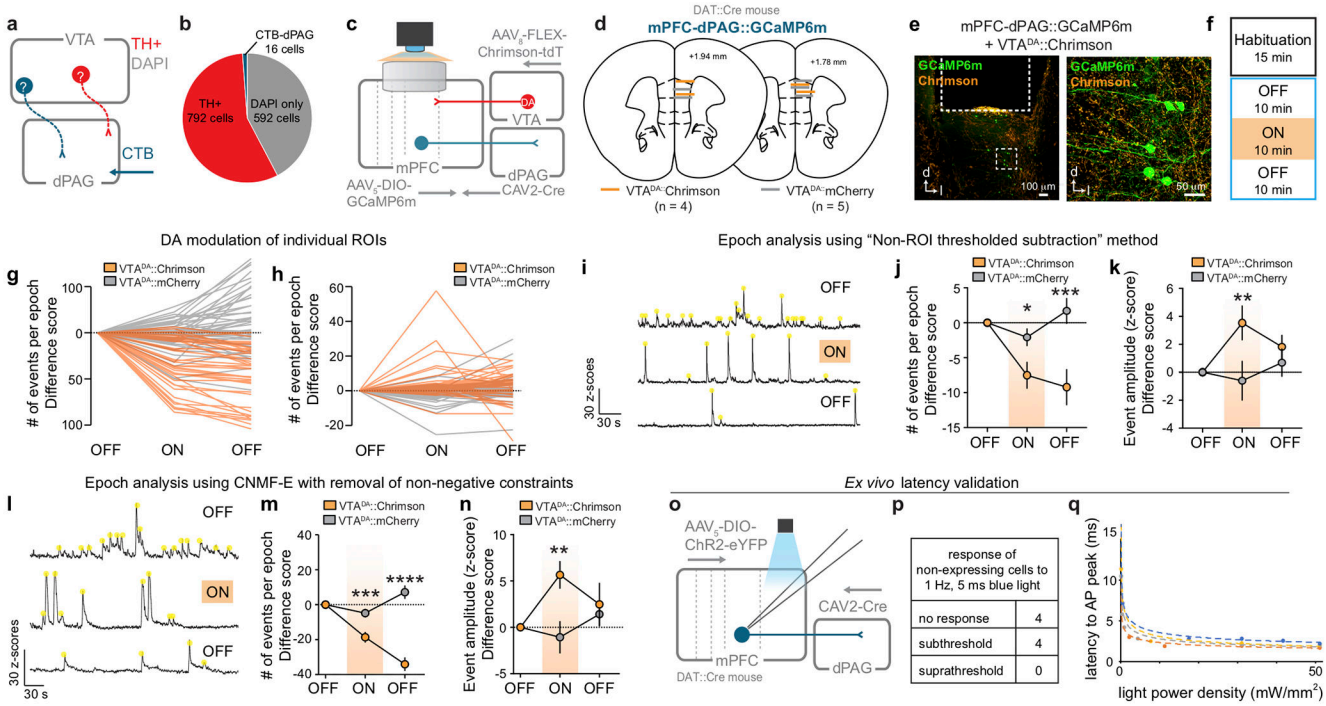

Extended Data Figure 8. Investigation of VTA projections to the dPAG for simultaneous epifluorescent imaging in mPFC-dPAG neurons and excitation of VTA^{DA} terminals.

(a) To verify that VTA neurons do not project to the dPAG (to allow for CAV-Cre mediated GCaMP6m expression in dPAG neurons and simultaneous expression of the excitatory opsin Chrimson in VTA^{DA} neurons in DAT::Cre mice) VTA slices were immunostained for tyrosine hydroxylase (TH) in rats injected with the retrograde tracer CTB in the dPAG. **(b)** Of 1,400 DAPI+ cells counted in the VTA, 792 (56%) were TH+, 16 (1.1%) were CTB+, and 0 were TH+ and CTB+. The lack of CTB+ cells suggests that VTA does not make a prominent projection to the dPAG. Of the retrogradely labeled cells observed in the VTA, none were TH+. **(c)** Schematic of strategy to simultaneously image fluorescent calcium activity in mPFC-dPAG::GCaMP6m neurons and activate VTA^{DA}-mPFC. **(d)** Histological verification of GRIN lens locations in the mPFC in mPFC-dPAG::GCaMP6m x VTA^{DA}::Chrimson subjects and control mPFC-dPAG::GCaMP6m x VTA^{DA}::mCherry subjects. **(e)** Representative confocal images of mPFC-dPAG::GCaMP6m and VTA^{DA}::Chrimson expression in the mPFC. **(f)** Schematic of experimental design. During the ON epoch, a 620 nm LED stimulated Chrimson expressing VTA^{DA}-mPFC (20 Hz, 60 p, 5 ms pulses, every 30 s). **(g)** Individual ROI transient frequency analyzed with CNMF-E. **(h)** Individual ROI transient amplitude analyzed with CNMF-E. **i-k,** Data analyzed using a non-ROI thresholded subtraction method (Chrimson: n = 4 mice, 44 ROIs; mCherry: n = 5 mice; 50 ROIs) **(i)** Representative traces from a mPFC-dPAG::GCaMP6m neuron during the OFF-ON-OFF recording epochs. Calcium transients (yellow dots) for each neuron were identified and quantified. **(j)** VTA^{DA}-mPFC stimulation decreased the average calcium event frequency per neuron, during both the ON and second OFF epochs (data normalized to first OFF epoch; two-way repeated measure ANOVA, $F_{2,184} = 9.209$, $p = 0.0002$, Bonferroni multiple comparisons tests, $p < 0.05$). **(k)** VTA^{DA}-mPFC stimulation increased the average

Author Manuscript Author Manuscript Author Manuscript Author Manuscript

calcium event amplitude per cell during the ON epoch, an effect that recovered in the second OFF epoch (data normalized to first OFF epoch; two-way repeated measure ANOVA, $F_{2,184} = 3.756$, $p = 0.0252$, Bonferroni multiple comparisons tests, Chrimson ON vs. mCherry ON *$p = 0.117$, Chrimson OFF2 vs. mCherry OFF2 ***$p < 0.0001$). **l-n,** Data analyzed using CNMF-E with removal of non-negative constraints (Chrimson: n = 4 mice, 44 ROIs; mCherry: n = 5 mice; 50 ROIs). **(l)** Representative traces from a mPFC-dPAG::GCaMP6m neuron during each 10 min OFF-ON-OFF recording epoch. Calcium transients (yellow dots) for each neuron were identified and quantified. **(m)** VTA^{DA}-mPFC stimulation decreased the average calcium event frequency per neuron, during both the ON and second OFF epochs (data normalized to first OFF epoch; two-way repeated measure ANOVA, $F_{2,184} = 43.62$, $p < 0.0001$, Bonferroni multiple comparisons tests, Chrimson ON vs. mCherry ON ***$p = 0.0003$, Chrimson OFF2 vs. mCherry OFF2 ***$p < 0.0001$). **(n)** VTA^{DA}-mPFC stimulation increased the average calcium event amplitude per cell during the ON epoch, an effect that recovered in the second OFF epoch (data normalized to first OFF epoch; two-way repeated measure ANOVA, $F_{2,184} = 3.50$, $p = 0.0322$, Bonferroni multiple comparisons tests, Chrimson ON vs. mCherry ON **$p = 0.0010$). **(o)** Schematic of viral strategy to optically manipulate ChR2-expressing VTA^{DA} terminals in the mPFC and record from mPFC-dPAG::ChR2 and non-expressing neighboring neurons with *ex vivo* electrophysiology. **(p)** Number of non-expressing cells with different responses to 1 Hz, 5 ms blue light delivery. **(q)** Latency to AP peak for all ChR2-expressing cells plotted against light power density. Error bars indicate ±SEM. The mouse brains in this figure were reproduced with permission from Paxinos and Franklin, 2004.

Author Manuscript Author Manuscript Author Manuscript Author Manuscript

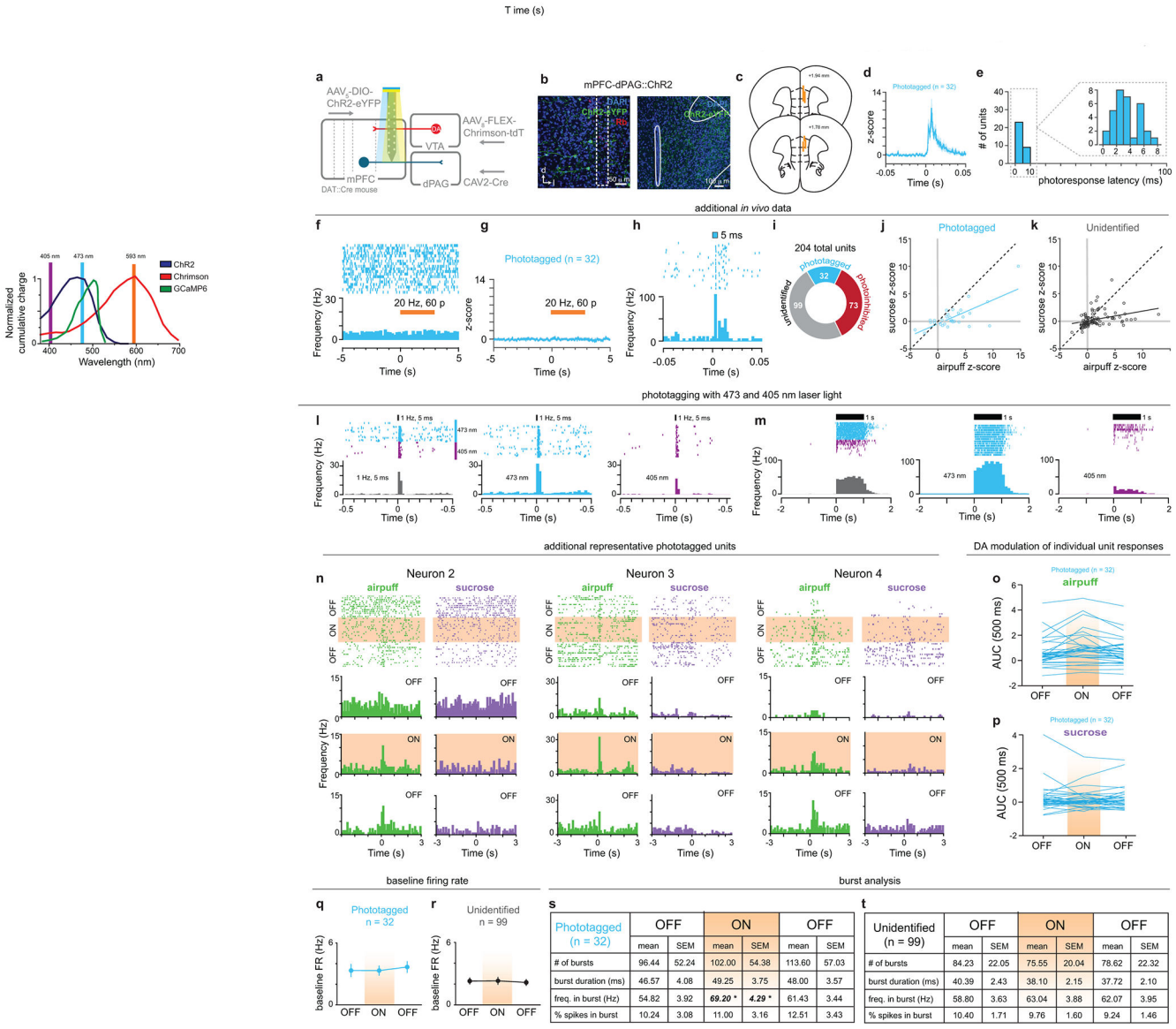

Phototagged (n = 32)	OFF		ON		OFF	
	mean	SEM	mean	SEM	mean	SEM
# of bursts	96.44	52.24	102.00	54.38	113.60	57.03
burst duration (ms)	46.57	4.08	49.25	3.75	48.00	3.57
freq. in burst (Hz)	54.82	3.92	***69.20*** *	***4.29*** *	61.43	3.44
% spikes in burst	10.24	3.08	11.00	3.16	12.51	3.43

Unidentified (n = 99)	OFF		ON		OFF	
	mean	SEM	mean	SEM	mean	SEM
# of bursts	84.23	22.05	75.55	20.04	78.62	22.32
burst duration (ms)	40.39	2.43	38.10	2.15	37.72	2.10
freq. in burst (Hz)	58.80	3.63	63.04	3.88	62.07	3.95
% spikes in burst	10.40	1.71	9.76	1.60	9.24	1.46

Extended Data Figure 9. Additional data for head-fixed electrophysiological recordings.

(a) Schematic of strategy to manipulate VTA^{DA} terminals in the mPFC and optically identify mPFC-dPAG::ChR2 neurons using *in vivo* head-fixed electrophysiology. **(b)** Representative image of recording track in the mPFC (Rb, red retrobeads) and ChR2-eYFP-expressing mPFC-dPAG neurons. Representative image of ChR2-eYFP-expressing terminals surrounding the PAG. **(c)** Histologically verified locations of recording tracks for *in vivo* head-fixed electrophysiology experiments. **(d)** Population z-score of all phototagged units aligned to 1 Hz, 5 ms pulse of 473 nm. **(e)** Photoresponse latencies showing < 8 ms response latency from all 32 mPFC-dPAG::ChR2 units. **(f)** PSTH from representative phototagged unit and **(g)** population z-score showing no response to 20 Hz, 60 pulses of 593 nm laser light used for VTA^{DA}::Chrimson terminal activation. **(h)** Representative peri-stimulus time PSTH of the firing rate in response to the onset of 5 ms pulse of 473 nm laser light used for phototagging. **(i)** 204 mPFC units were recorded (n = 3 mice, 5 recording sessions) and 32

Author Manuscript Author Manuscript Author Manuscript Author Manuscript

phototagged units were identified as mPFC-dPAG projectors (blue), 73 were photoinhibited (red), and 99 remained unidentified (black). **(j)** Neural response magnitudes to airpuff (x-axis) and sucrose (y-axis) in phototagged (blue) and **(k)** unidentified (black) populations. **l-m,** In a subset of mice, both 405 and 473 nm laser light were used for phototagging. **(l)** Representative phototagged unit showing faithful responses to 1 Hz, 5 ms pulses of both 473 and 405 nm light. **(m)** Representative phototagged unit showing blunted response to 1 s of 405 nm, compared to 473 nm light. **(n)** Representative PSTHs of photoidentified mPFC-dPAG units aligned to airpuff (green) and sucrose (purple). Histograms show neural responses in the OFF-ON-OFF epochs. **(o)** Individual neural responses [AUC (0 – 500 ms post-stimulus presentation)] of every phototagged unit (n = 32 units) to airpuff and **(p)** sucrose in each of the three recording epochs (OFF-ON-OFF). **(q)** VTA dopamine terminal stimulation in the mPFC did not change the baseline firing rate (FR, Hz) in the 3 s pre-stimulus windows in the phototagged (Friedman Test, $X^2(2) = 2.472$ $p = 0.2905$) or **(r)** unidentified (Friedman Test, $X^2(2) = 0.4242$ $p = 0.8089$) populations. **(s)** VTA^{DA} terminal activation increased the frequency within a burst in the phototagged population. **(t)** VTA^{DA} terminal activation did not affect burst characteristics in the unidentified population. Error bars indicate ±SEM. The mouse brains in this figure were reproduced with permission from Paxinos and Franklin, 2004.

Author Manuscript Author Manuscript Author Manuscript Author Manuscript

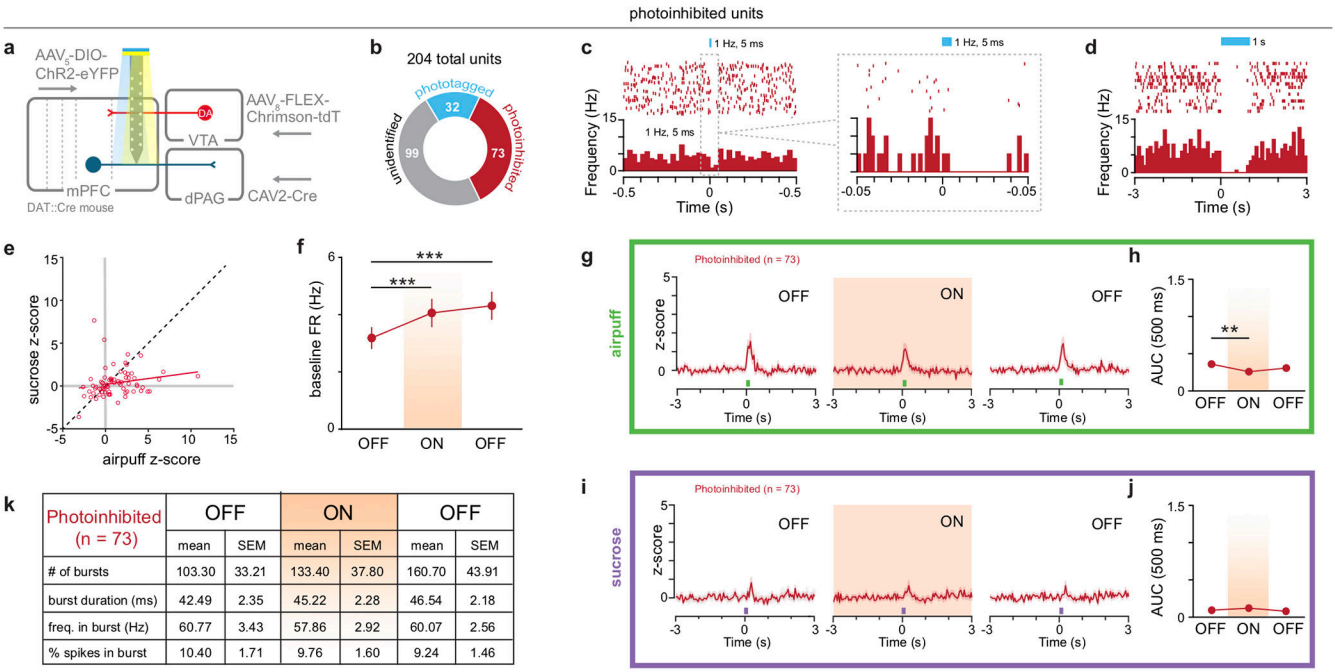

Photoinhibited (n = 73)	OFF		ON		OFF	
	mean	SEM	mean	SEM	mean	SEM
# of bursts	103.30	33.21	133.40	37.80	160.70	43.91
burst duration (ms)	42.49	2.35	45.22	2.28	46.54	2.18
freq. in burst (Hz)	60.77	3.43	57.86	2.92	60.07	2.56
% spikes in burst	10.40	1.71	9.76	1.60	9.24	1.46

Extended Data Figure 10. Photoinhibited

(a) Schematic of strategy to manipulate VTA^{DA} terminals in the mPFC and optically identify mPFC-dPAG::ChR2 neurons using *in vivo* head-fixed electrophysiology (n = 3 mice, 5 recording sessions). **(b)** 35.8% of recorded units (73/204) were photoinhibited. **(c)** Representative PSTHs of a photoinhibited unit in response to 1 Hz, 5 ms and **(d)** 1 s of 473 nm light. **(e)** Neural response magnitudes to airpuff (x-axis) and sucrose (y-axis) in photoinhibited (red) population. **(f)** VTA dopamine terminal stimulation in the mPFC increased the baseline firing rate (FR, Hz) in the 3 s pre-stimulus windows in the photoinhibited population (n = 73 units) during the ON and second OFF epochs (Friedman Test, $X^2(2) = 16.22$; $p = 0.0003$; Dunn's multiple comparisons tests, $p > 0.05$). **(g)** Population z-score of photoinhibited units aligned to airpuff in each of the recording epochs. **(h)** In photoinhibited neurons, VTA^{DA} terminal stimulation attenuated neural responses to airpuff (Friedman Test, $X^2(2) = 8.329$, $p = 0.0155$, Dunn's multiple comparisons tests, $p < 0.05$). **(i)** Population z-score of photoinhibited units aligned to sucrose in each of the recording epochs. **(j)** In photoinhibited neurons, VTA^{DA} terminal stimulation did not affect neural responses to sucrose (Friedman Test, $X^2(2) = 0.4492$, $p = 0.7988$, Dunn's multiple comparisons tests, $p > 0.05$). **(k)** VTA^{DA} terminal activation did not affect burst characteristics in the photoinhibited population. Error bars and shading represent ±SEM.

Supplementary Material

Refer to Web version on PubMed Central for supplementary material.

ACKNOWLEDGMENTS

We thank Drs. Ilana Witten, Courtney Cameron, Nathan Parker, Malavika Murugan, Pengcheng Zhou and Liam Paninski for advice and code for CNMF-E analysis. We thank Drs. Mark Schnitzer and Denise Cai for advice regarding endoscopic imaging. We thank Yi-Ning Leow, Andrew Shea, & Noa Golan for histological assistance.

Author Manuscript Author Manuscript Author Manuscript Author Manuscript

We appreciate Dr. Natsuko Imamura and Christopher Leppla for technical training. We recognize the generosity of the Genetically-Encoded Neuronal Indicator and Effector (GENIE) program, the Janelia Farm Research Campus, Drs. Vivek Jayaraman, Rex A. Kerr, Douglas S. Kim, Loren L. Looger, Karel Svoboda for providing GCaMP6m. We acknowledge Inscopix, Inc. for a scientific collaboration and providing early access to nVoke and Lara Cardy and Dr. Alice Stamatakis of Inscopix, Inc. for technical assistance. We thank Dr. Eric J. Kremer for providing CAV2-Cre vector, UNC vector core for ChR2, NpHR, and ChrimsonR vectors, and University of Pennsylvania vector core for GCaMP6m packaging. We recognize Dr. Rachel Neve (formerly at the Gene Transfer Core Facility at MIT, now at Massachusetts General Hospital) for packaging the AAV-DIO-synaptophysin-mCherry construct. Finally, we thank Dr. Jill Crittenden for donating D1-TdTomato/D2-GFP mice and Dr. Teruhiro Okuyama for donating Drd1a-Cre and Drd2-Cre mice.

REFERENCES

1. Arnsten AF T. Stress signalling pathways that impair prefrontal cortex structure and function. Nat. Rev. Neurosci. 10, 410 (2009). [PubMed: 19455173]
2. Miller EK & Cohen JD An Integrative Theory of Prefrontal Cortex Function. Annu. Rev. Neurosci. 24, 167–202 (2001). [PubMed: 11283309]
3. Cohen JD, Braver TS & Brown JW Computational perspectives on dopamine function in prefrontal cortex. Curr. Opin. Neurobiol. 12, 223–229 (2002). [PubMed: 12015241]
4. Kroener S, Chandler LJ, Phillips PEM & Seamans JK Dopamine modulates persistent synaptic activity and enhances the signal-to-noise ratio in the prefrontal cortex. PloS One 4, e6507 (2009). [PubMed: 19654866]
5. Rolls ET, Loh M, Deco G & Winterer G Computational models of schizophrenia and dopamine modulation in the prefrontal cortex. Nat. Rev. Neurosci. 9, 696–709 (2008). [PubMed: 18714326]
6. Winterer G & Weinberger DR Genes, dopamine and cortical signal-to-noise ratio in schizophrenia. Trends Neurosci. 27, 683–690 (2004). [PubMed: 15474169]
7. Popescu AT, Zhou MR & Poo M-M Phasic dopamine release in the medial prefrontal cortex enhances stimulus discrimination. Proc. Natl. Acad. Sci. U. S. A. 113, E3169–3176 (2016). [PubMed: 27185946]
8. Noudoost B & Moore T Control of visual cortical signals by prefrontal dopamine. Nature 474, 372–375 (2011). [PubMed: 21572439]
9. Williams GV & Goldman-Rakic PS Modulation of memory fields by dopamine D1 receptors in prefrontal cortex. Nature 376, 572–575 (1995). [PubMed: 7637804]
10. Burgos-Robles A et al. Amygdala inputs to prefrontal cortex guide behavior amid conflicting cues of reward and punishment. Nat. Neurosci. 20, 824–835 (2017). [PubMed: 28436980]
11. Euston DR, Gruber AJ & McNaughton BL The role of medial prefrontal cortex in memory and decision making. Neuron 76, 1057–1070 (2012). [PubMed: 23259943]
12. Kim CK et al. Simultaneous fast measurement of circuit dynamics at multiple sites across the mammalian brain. Nat. Methods 13, 325–328 (2016). [PubMed: 26878381]
13. Lammel S, Ion DI, Roeper J & Malenka RC Projection-specific modulation of dopamine neuron synapses by aversive and rewarding stimuli. Neuron 70, 855–862 (2011). [PubMed: 21658580]
14. Abercrombie ED, Keefe KA, DiFrischia DS & Zigmond MJ Differential effect of stress on in vivo dopamine release in striatum, nucleus accumbens, and medial frontal cortex. J. Neurochem. 52, 1655–1658 (1989). [PubMed: 2709017]
15. Thierry AM, Tassin JP, Blanc G & Glowinski J Selective activation of mesocortical DA system by stress. Nature 263, 242–244 (1976). [PubMed: 958479]
16. Mantz J, Thierry AM & Glowinski J Effect of noxious tail pinch on the discharge rate of mesocortical and mesolimbic dopamine neurons: selective activation of the mesocortical system. Brain Res. 476, 377–381 (1989). [PubMed: 2702475]
17. Finlay JM, Zigmond MJ & Abercrombie ED Increased dopamine and norepinephrine release in medial prefrontal cortex induced by acute and chronic stress: effects of diazepam. Neuroscience 64, 619–628 (1995). [PubMed: 7715775]
18. Heien MLAV, Phillips PEM, Stuber GD, Seipel AT & Wightman RM Overoxidation of carbon-fiber microelectrodes enhances dopamine adsorption and increases sensitivity. The Analyst 128, 1413–1419 (2003). [PubMed: 14737224]

Author Manuscript Author Manuscript Author Manuscript Author Manuscript

19. Bandler R & Carrive P Integrated defence reaction elicited by excitatory amino acid microinjection in the midbrain periaqueductal grey region of the unrestrained cat. Brain Res. 439, 95–106 (1988). [PubMed: 3359200]
20. Deng H, Xiao X & Wang Z Periaqueductal Gray Neuronal Activities Underlie Different Aspects of Defensive Behaviors. J. Neurosci. Off. J. Soc. Neurosci. 36, 7580–7588 (2016).
21. Tovote P et al. Midbrain circuits for defensive behaviour. Nature 534, 206–212 (2016). [PubMed: 27279213]
22. Franklin TB et al. Prefrontal cortical control of a brainstem social behavior circuit. bioRxiv 073734 (2016). doi:10.1101/073734
23. Murugan M et al. Combined Social and Spatial Coding in a Descending Projection from the Prefrontal Cortex. Cell 171, 1663–1677.e16 (2017). [PubMed: 29224779]
24. Otis JM et al. Prefrontal cortex output circuits guide reward seeking through divergent cue encoding. Nature 543, 103–107 (2017). [PubMed: 28225752]
25. Britt JP et al. Synaptic and behavioral profile of multiple glutamatergic inputs to the nucleus accumbens. Neuron 76, 790–803 (2012). [PubMed: 23177963]
26. Ghosh KK et al. Miniaturized integration of a fluorescence microscope. Nat. Methods 8, 871–878 (2011). [PubMed: 21909102]
27. Chen T-W et al. Ultrasensitive fluorescent proteins for imaging neuronal activity. Nature 499, 295–300 (2013). [PubMed: 23868258]
28. Zhou P et al. Efficient and accurate extraction of in vivo calcium signals from microendoscopic video data. eLife 7, (2018).
29. Klapoetke NC et al. Independent optical excitation of distinct neural populations. Nat. Methods 11, 338–346 (2014). [PubMed: 24509633]
30. Beyeler A et al. Divergent routing of positive and negative information from the amygdala during memory retrieval. Neuron 90, 348–361 (2016). [PubMed: 27041499]

METHODS REFERENCES

31. Nagel G et al. Channelrhodopsin-2, a directly light-gated cation-selective membrane channel. Proc. Natl. Acad. Sci. 100, 13940–13945 (2003). [PubMed: 14615590]
32. Zhang F, Wang L-P, Boyden ES & Deisseroth K Channelrhodopsin-2 and optical control of excitable cells. Nat. Methods 3, 785–792 (2006). [PubMed: 16990810]
33. Gradinaru V, Thompson KR & Deisseroth K eNpHR: a Natronomonas halorhodopsin enhanced for optogenetic applications. Brain Cell Biol. 36, 129–139 (2008). [PubMed: 18677566]
34. Schobert B & Lanyi JK Halorhodopsin is a light-driven chloride pump. J. Biol. Chem. 257, 10306–10313 (1982). [PubMed: 7107607]
35. Klapoetke NC et al. Independent optical excitation of distinct neural populations. Nat. Methods 11, 338–346 (2014). [PubMed: 24509633]
36. Chen T-W et al. Ultrasensitive fluorescent proteins for imaging neuronal activity. Nature 499, 295–300 (2013). [PubMed: 23868258]
37. Akerboom J et al. Genetically encoded calcium indicators for multi-color neural activity imaging and combination with optogenetics. Front. Mol. Neurosci. 6, 2 (2013). [PubMed: 23459413]
38. Kremer EJ, Boutin S, Chillon M & Danos O Canine Adenovirus Vectors: an Alternative for Adenovirus-Mediated Gene Transfer. J. Virol. 74, 505–512 (2000). [PubMed: 10590140]
39. Witten IB et al. Recombinase-driver rat lines: tools, techniques, and optogenetic application to dopamine-mediated reinforcement. Neuron 72, 721–733 (2011). [PubMed: 22153370]
40. Tsai H-C et al. Phasic Firing in Dopaminergic Neurons Is Sufficient for Behavioral Conditioning. Science 324, 1080–1084 (2009). [PubMed: 19389999]
41. Nieh EH et al. Inhibitory Input from the Lateral Hypothalamus to the Ventral Tegmental Area Disinhibits Dopamine Neurons and Promotes Behavioral Activation. Neuron 90, 1286–1298 (2016). [PubMed: 27238864]
42. Sparta DR et al. Construction of implantable optical fibers for long-term optogenetic manipulation of neural circuits. Nat. Protoc. 7, 12–23 (2012).

Author Manuscript Author Manuscript Author Manuscript Author Manuscript

43. Robinson DL, Venton BJ, Heien MLAV & Wightman RM Detecting Subsecond Dopamine Release with Fast-Scan Cyclic Voltammetry in Vivo. Clin. Chem. 49, 1763–1773 (2003). [PubMed: 14500617]
44. Heien MLAV, Phillips PEM, Stuber GD, Seipel AT & Wightman RM Overoxidation of carbon-fiber microelectrodes enhances dopamine adsorption and increases sensitivity. The Analyst 128, 1413–1419 (2003). [PubMed: 14737224]
45. Keithley RB & Wightman RM Assessing Principal Component Regression Prediction of Neurochemicals Detected with Fast-Scan Cyclic Voltammetry. ACS Chem. Neurosci. 2, 514–525 (2011). [PubMed: 21966586]
46. Keithley RB, Mark Wightman R & Heien ML Multivariate concentration determination using principal component regression with residual analysis. TrAC Trends Anal. Chem. 28, 1127–1136 (2009).
47. Burgos-Robles A et al. Amygdala inputs to prefrontal cortex guide behavior amid conflicting cues of reward and punishment. Nat. Neurosci. 20, 824–835 (2017). [PubMed: 28436980]
48. Conte WL, Kamishina H & Reep RL Multiple neuroanatomical tract-tracing using fluorescent Alexa Fluor conjugates of cholera toxin subunit B in rats. Nat. Protoc. 4, 1157–1166 (2009). [PubMed: 19617887]
49. Zhuang X, Masson J, Gingrich JA, Rayport S & Hen R Targeted gene expression in dopamine and serotonin neurons of the mouse brain. J. Neurosci. Methods 143, 27–32 (2005). [PubMed: 15763133]
50. Ghosh KK et al. Miniaturized integration of a fluorescence microscope. Nat. Methods 8, 871–878 (2011). [PubMed: 21909102]
51. Resendez SL et al. Visualization of cortical, subcortical and deep brain neural circuit dynamics during naturalistic mammalian behavior with head-mounted microscopes and chronically implanted lenses. Nat. Protoc. 11, 566–597 (2016). [PubMed: 26914316]
52. Jennings JH et al. Visualizing hypothalamic network dynamics for appetitive and consummatory behaviors. Cell 160, 516–527 (2015). [PubMed: 25635459]
53. Ziv Y et al. Long-term dynamics of CA1 hippocampal place codes. Nat. Neurosci. 16, 264–266 (2013). [PubMed: 23396101]
54. Zhou P et al. Efficient and accurate extraction of in vivo calcium signals from microendoscopic video data. eLife 7, (2018).
55. Murugan M et al. Combined Social and Spatial Coding in a Descending Projection from the Prefrontal Cortex. Cell 171, 1663–1677.e16 (2017). [PubMed: 29224779]
56. Otis JM et al. Prefrontal cortex output circuits guide reward seeking through divergent cue encoding. Nature 543, 103–107 (2017). [PubMed: 28225752]
57. Mukamel EA, Nimmerjahn A & Schnitzer MJ Automated Analysis of Cellular Signals from Large-Scale Calcium Imaging Data. Neuron 63, 747–760 (2009). [PubMed: 19778505]
58. Novák P & Zahradník I Q-method for high-resolution, whole-cell patch-clamp impedance measurements using square wave stimulation. Ann. Biomed. Eng. 34, 1201–1212 (2006). [PubMed: 16786392]
59. Beyeler A et al. Divergent Routing of Positive and Negative Information from the Amygdala during Memory Retrieval. Neuron 90, 348–361 (2016). [PubMed: 27041499]
60. Burgos-Robles A, Vidal-Gonzalez I, Santini E & Quirk GJ Consolidation of Fear Extinction Requires NMDA Receptor-Dependent Bursting in the Ventromedial Prefrontal Cortex. Neuron 53, 871–880 (2007). [PubMed: 17359921]
61. Paxinos G & Watson C The rat brain in stereotaxic coordinates: hard cover edition. (Academic press, 2006).
62. Paxinos G & Franklin KB The mouse brain in stereotaxic coordinates. (Gulf Professional Publishing, 2004).

Author Manuscript Author Manuscript Author Manuscript Author Manuscript

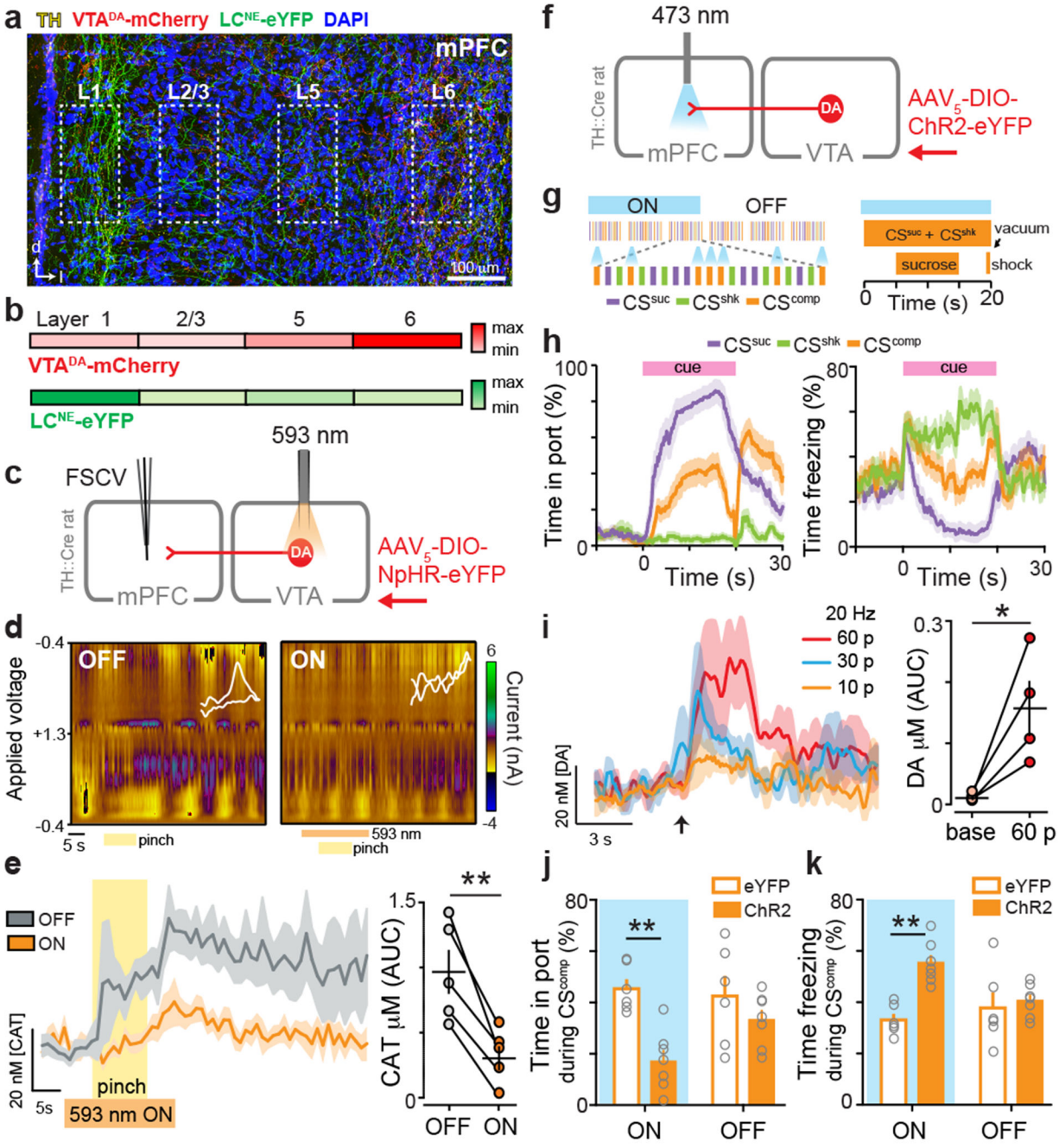

Figure 1. Tail pinch evokes rapid DA release in the mPFC and DA biases behavior towards aversion during stimulus competition.

(a) VTA^{DA} and LC^{NE} terminals in the mPFC. **(b)** VTA^{DA} terminals were densest in deep layers. LC^{NE} terminals were densest in superficial layers (n = 3 mice). **(c)** Strategy to verify dependence of pinch-evoked catecholamine neurotransmission (CAT) on VTA^{DA} neurons. **(d)** Representative false color plots showing tail pinch evoked CAT before and during VTA^{DA} inhibition (593 nm laser light, 20 s) (n = 5 rats). **(e)** Photoinhibition of VTA^{DA} neurons attenuated tail-pinch-evoked CAT release, evident in the average traces (left) and

Author Manuscript Author Manuscript Author Manuscript Author Manuscript

concentration quantification (right) (two-tailed paired t-test, $t(4) = 5.884$, $^{**}p = 0.004$). **(f)** Strategy for manipulating DA release in the mPFC. **(g)** Schematic of competition task. During "competition" sessions, in addition to sucrose (CS^{suc}, purple) and shock (CS^{shk}, green) trials, CS^{suc} and CS^{shk} were co-presented as competition trials (CS^{comp}. orange). During "ON" sessions, VTA^{DA}-mPFC was activated (473 nm, 20 Hz, 60 pulses, every 5 s) during the CS^{comp} trials. During "OFF", light was not delivered. **(h)** Percent time spent in the reward port and freezing during each trial type (n = 13 rats). **(i)** Evoked DA release in the mPFC following 20 Hz optical activation of VTA^{DA}::ChR2-mCherry (n = 4 rats; 60 pulses: two-tailed paired t-test, $t(3) = 3.72$, $^{*}p = 0.034$). **(j)** Average time spent in the reward port during CS^{comp} ON trials was lower in ChR2 rats (n = 7 rats; closed bars) compared with eYFP (n = 6 rats; open bars) (repeated measures two-way ANOVA, $F_{1,11} = 8.13$, $p = 0.0157$, Bonferroni multiple comparisons tests $^{**}p = 0.0025$). **(k)** Average time spent freezing during CS^{comp} ON trials was greater in ChR2 rats compared with eYFP (repeated measures two-way ANOVA, $F_{1,11} = 13.29$, $p = 0.0039$, Bonferroni multiple comparisons tests $^{**}p = 0.0013$). Error bars and shading represent ±SEM. AUC = area under the curve.

Author Manuscript Author Manuscript Author Manuscript Author Manuscript

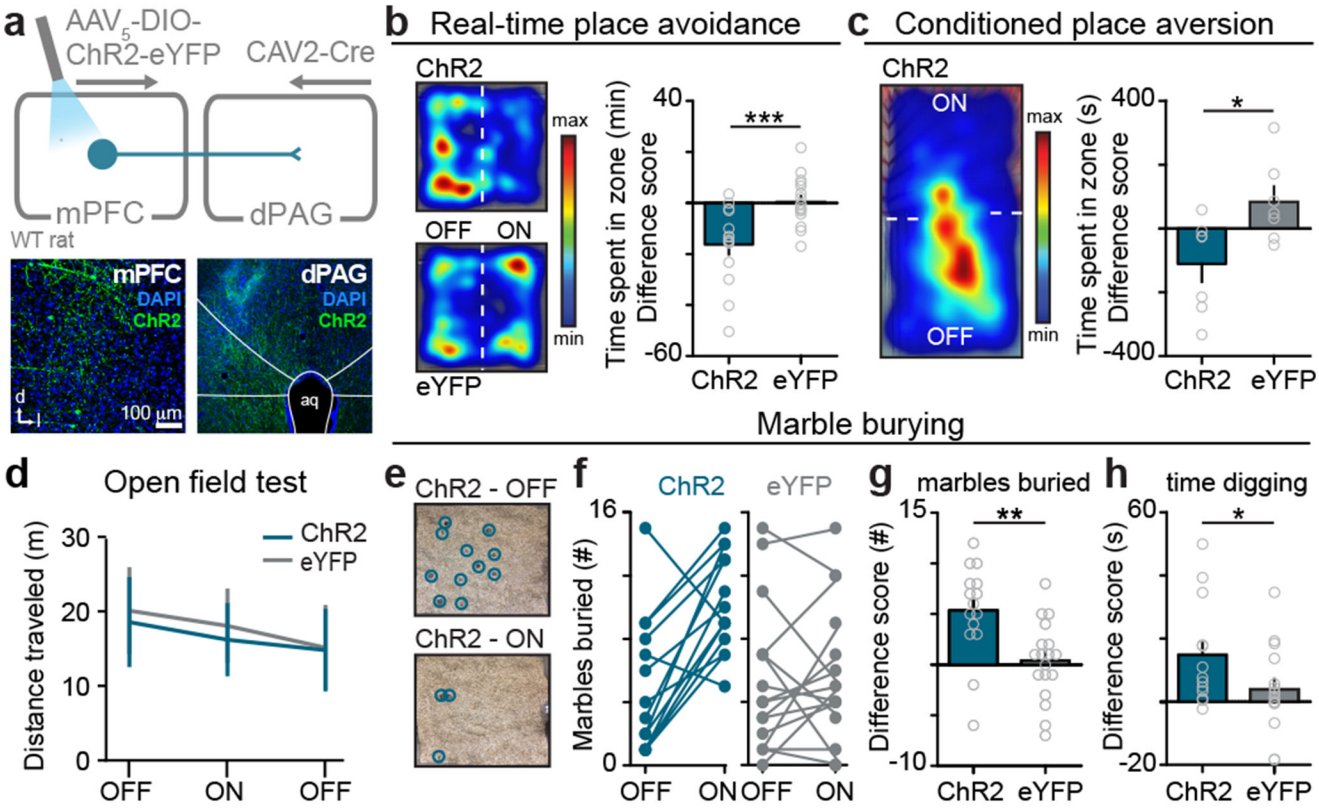

Figure 2. The mPFC promotes aversion through projections to the dPAG.

(a) Viral strategy to activate mPFC neurons projecting to the dPAG (top). Representative images of the mPFC and dPAG (bottom). **(b)** Representative locomotor heatmaps of mPFC-dPAG::ChR2 and mPFC-dPAG::eYFP subjects in RTPA (left). Activation of mPFC-dPAG neurons resulted in RTPA in mPFC-dPAG::ChR2 animals (n = 15 rats), compared with mPFC-dPAG::eYFP controls (n = 17 rats) (right) [minutes spent in the ON zone – OFF zone] (two-tailed unpaired t-test, t(30) = 3.902, ***p = 0.0005). **(c)** Representative locomotor heatmap of mPFC-dPAG::ChR2 subject on test day of CPA (left). Activation of mPFC-dPAG neurons produced CPA in mPFC-dPAG::ChR2 animals (n = 7 rats), compared with mPFC-dPAG::eYFP controls (n = 7 rats) (right) [minutes spent in the ON zone – OFF zone] (two-tailed unpaired t-test, t(12) = 2.638, *p = 0.0217). **(d)** Optical activation of mPFC-dPAG::ChR2 did not change locomotor activity (ChR2 n = 15; eYFP n = 18; distance traveled, two-way repeated measures ANOVA, group x epoch interaction, $F_{2,62} = 0.94$, p = 0.3957). **(e)** Representative arena of mPFC-dPAG::ChR2 animal after marble burying assay when laser stimulation was OF or ON. **(f)** Number of marbles buried in ON and OFF conditions for mPFC-dPAG::ChR2 and mPFC-dPAG::eYFP rats. **(g)** Optogenetic stimulation of mPFC-dPAG neurons resulted in a greater change in marbles buried by mPFC-dPAG::ChR2 (n = 15 rats) compared to mPFC-dPAG::eYFP (n = 18 rats) [# of marbles buried during ON session – OFF session] (two-tailed unpaired t-test, t(31) = 3.341, **p = 0.0022). **(h)** mPFC-dPAG::ChR2 (n = 13 rats) spent more time digging during optical stimulation compared with mPFC-dPAG::eYFP (n = 16 rats) [ON-OFF] (one-tailed unpaired t-test, t(27) = 1.961, *p = 0.0301). Error bars indicate ±SEM.

Author Manuscript Author Manuscript Author Manuscript Author Manuscript

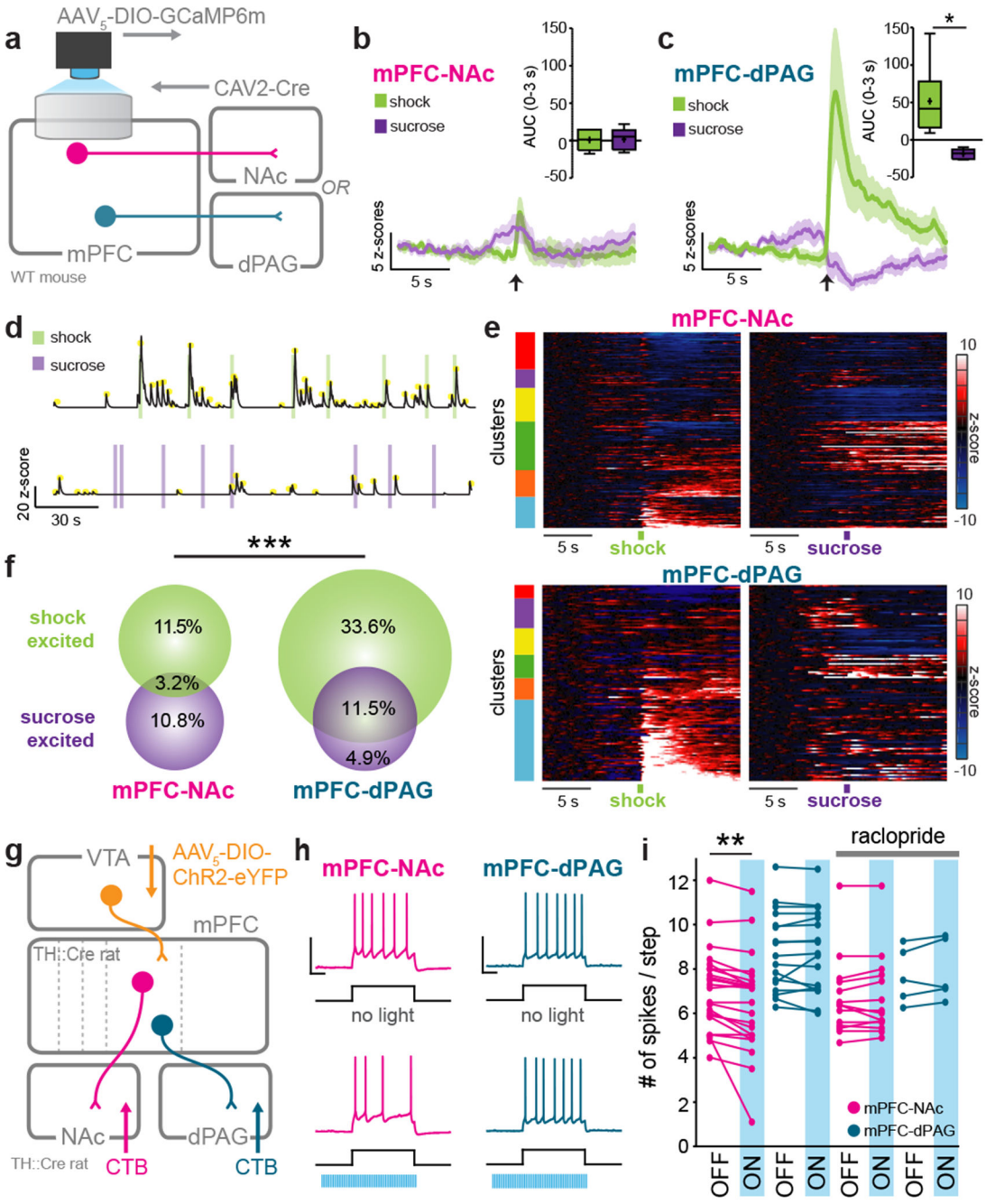

Figure 3. mPFC-dPAG neurons preferentially respond to aversive stimuli.

(a) Strategy for recording calcium activity in mPFC-dPAG and mPFC-NAc. **(b)** Bulk fluorescence aligned to shock and sucrose bout in mPFC-NAc::GCaMP6m (n = 5 mice). mPFC-NAc::GCaMP6m responses to sucrose did not differ from responses to shock (0-3 s AUC, two-tailed paired t-test, t(4)=0.1482, p = 0.8893). **(c)** Bulk fluorescence in mPFC-dPAG::GCaMP6m neurons (n = 6 mice). mPFC-NAc::GCaMP6m calcium responses to shock were greater than to sucrose (0-3 s AUC, two-tailed paired t-test, t(5)=3.743, *p = 0.0134). **(d)** Signals were extracted from individual ROIs. Individual transients indicated by

Author Manuscript Author Manuscript Author Manuscript Author Manuscript

yellow dots. **(e)** Average traces per ROI aligned to shock or sucrose for each population. Agglomerative clustering results are shown in the bars on the left of each heatmap. **(f)** The distribution of shock and sucrose excited cells for mPFC-dPAG::GCaMP6m (n = 118 ROIs) was different from mPFC-NAc::GCaMP6m (n = 169 ROIs) (chi square, $X^2 = 14.76$, ***p = 0.0006). **(g)** Viral strategy to manipulate VTA^{DA}-mPFC::ChR2 and record from dPAG- or NAc-projectors *ex vivo*. **(h)** Representative traces from mPFC-NAc and mPFC-dPAG neurons during a current step without and with activation of VTA^{DA}-mPFC (470 nm, 20 Hz, 60 pulses). **(i)** Optical activation of VTA^{DA}-mPFC did not influence mPFC-dPAG (n = 17 cells) but decreased the number of spikes per step in mPFC-NAc (n = 24 cells), an effect not observed with D2-receptor antagonism (mPFC-dPAG n = 5 cells; mPFC-NAc n = 14 cells) (two-tailed repeated measures ANOVA, $F_{3,56} = 5.531$, p = 0.0027, Bonferroni multiple comparisons tests, mPFC-NAc OFF vs. ON, **p < 0.0001). Error bars and shading represent ±SEM. AUC = area under the curve. Scale bars (electrophysiology) = 500 ms (x-axis), 50 mV (y-axis). Whiskers = minima and maxima. Boxes = lower and upper quartile. Center line = median. + = mean.

Author Manuscript Author Manuscript Author Manuscript Author Manuscript

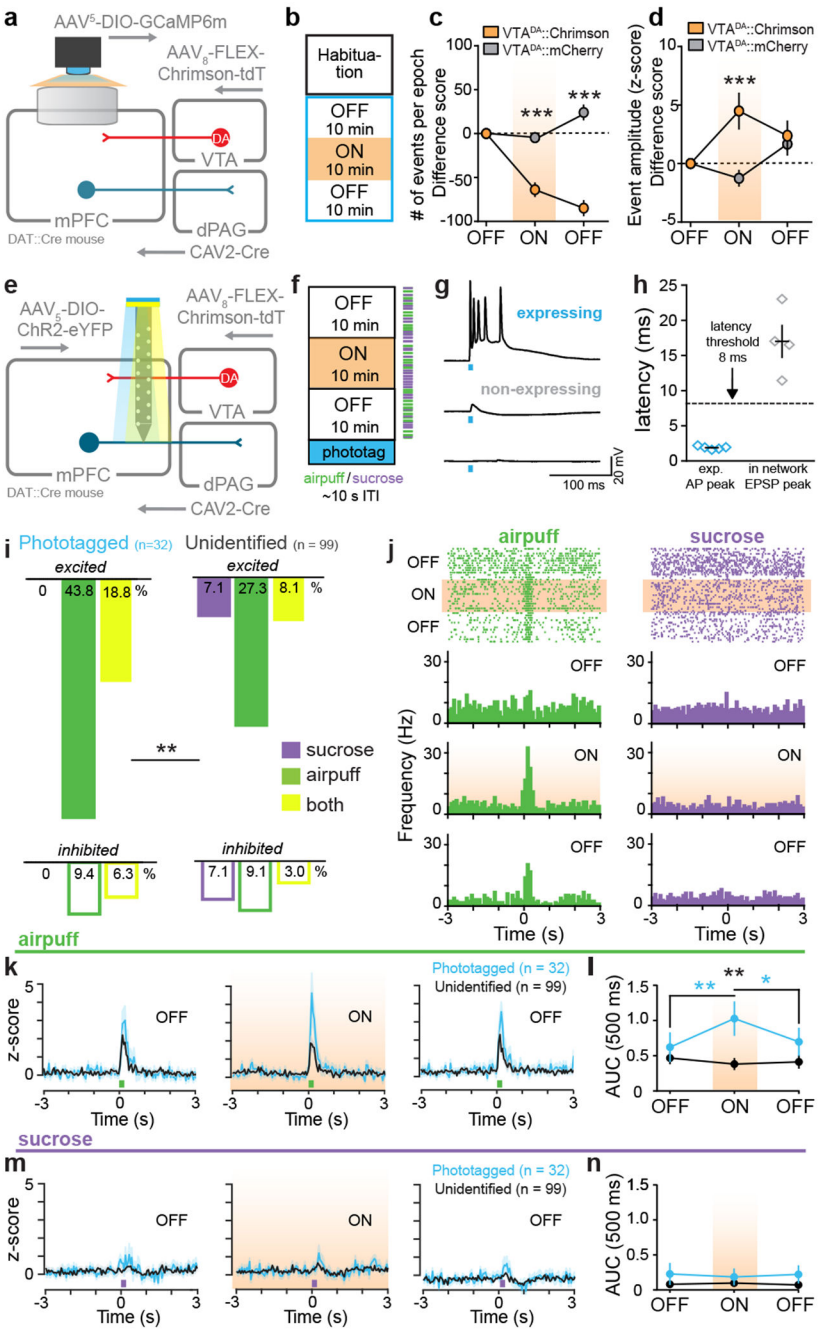

Figure 4. DA enhances SNR of mPFC-dPAG neural responses to aversive stimuli.

(a) Strategy to image activity in mPFC-dPAG::GCaMP6m and activate VTA^{DA}-mPFC *in vivo*. **(b)** During the ON epoch, 620 nm stimulated VTA^{DA}-mPFC::Chrimson (20 Hz, 60 p, every 30 s). **(c)** VTA^{DA}-mPFC stimulation decreased event frequency (two-way repeated measure ANOVA, $F_{2,184} = 57.61$, $p < 0.0001$, Bonferroni multiple comparisons tests, ***$p < 0.0001$) (Chrimson n = 4 mice, 44 ROIs) (mCherry control, n = 5 mice, 50 ROIs). **(d)** VTA^{DA}-mPFC stimulation increased event amplitude (two-way repeated measure ANOVA, $F_{2,184} = 5.843$, $p = 0.0035$, Bonferroni multiple comparisons tests, (***$p < 0.0001$). **(e)**

Author Manuscript Author Manuscript Author Manuscript Author Manuscript

Strategy to manipulate VTA^{DA}-mPFC and identify mPFC-dPAG::ChR2 using *in vivo* electrophysiology. **(f)** During the ON epoch, 593 nm stimulated VTA^{DA}–mPFC::Chrimson (20 Hz, 60 pulses, every 30 s). Mice received random sucrose and airpuff deliveries. **(g)** Representative traces from a ChR2-expressing and non-expressing cells in response to blue light *ex vivo.* **(h)** Latency to action potential (AP) peak for ChR2-expressing (n = 5 cells) and to EPSP peak for non-expressing (n = 4 cells) neurons. **(i)** Excitatory response patterns were different between populations (chi square, $X^2 = 9.52$, p = 0.0016). **(j)** Representative peri-stimulus time histogram (PSTH) of mPFC-dPAG. **(k)** Population z-score for phototagged and unidentified units aligned to airpuff. **(l)** VTA^{DA}-mPFC enhanced airpuff responses in phototagged, but not unidentified neurons (two-way repeated measure ANOVA, $F_{2,258} = 6.196$, p = 0.0024, Bonferroni multiple comparisons tests, phototagged OFF1 vs. ON **p = 0.0014, phototagged ON vs. OFF2 *p = 0.0091, unidentified OFF1 vs. ON vs. OFF2 p > 0.05; phototagged ON vs. unidentified ON **p = 0.0012)). **(m)** Population z-score for phototagged and unidentified units aligned to sucrose. **(n)** VTA^{DA}-mPFC did not change responses to sucrose (two-way repeated measure ANOVA, $F_{2,258} = 0.4420$, p = 0.6432). Error bars and shading represent ±SEM. AUC = area under the curve.